https://doi.org/10.5194/nhess-2021-342
Preprint. Discussion started: 25 November 2021

Natural Hazards and Earth System Sciences
Discussions

Characteristics of hail hazard in South Africa based on satellite detection of convective storms

Heinz Jürgen Punge[1], Kristopher M. Bedka[2], Michael Kunz[1], Sarah D. Bang[3], and Kyle F. Itterly[4]

[1]Karlsruhe Institute of Technology, Institute of Meteorology and Climate Research, Karlsruhe, Germany
[2]NASA Langley Research Center, Science Directorate, Climate Science Branch, Hampton, VA, USA
[3]NASA Marshall Space Flight Center (ST-11), Huntsville, AL, USA
[4]Science Systems and Applications Inc., Hampton, Virginia USA

Correspondence: Michael Kunz (michael.kunz@kit.edu)

Abstract. Accurate estimates of hail risk to fixed and mobile assets such as crops, infrastructure and vehicles are required for both insurance pricing and preventive measures. Here we present an event catalog to describe hail hazard in South Africa guided by 14 years of geostationary satellite observations of convective storms. Overshooting cloud tops have been detected, grouped and tracked to describe the spatio-temporal extent of potential hail events. It is found that hail events concentrate mainly in the southeast of the country, along the Highveld and the eastern slopes. Events are most frequent from mid-November through February and peak in the afternoon, between 13 and 17 UTC. Multivariate stochastic modeling of event properties yields an event catalog spanning 25 000 years, aiming to estimate, in combination with vulnerability and exposure data, hail damage for return periods of 200 years.

1 Introduction

Damage from hailfall is a significant contribution to natural hazards losses in many parts of the world, including South Africa, and growing research activity has opened up opportunities to estimate risk for the insurance sector (Allen et al., 2020). In South Africa, hail has long been known to generate large amounts of damage to agriculture – around two percent of the value of products (Carte, 1977) – and forestry (Smith et al., 2002; Wingfield and Swart, 1994). Events with severe hail damage to housing, vehicles and infrastructure like the one on November 28, 2013 (total loss SAR 1.4 bn, Powell and Burger, 2014; Visser, 2014) are numerous (e.g., Perry, 1995). Still, in comparison to other natural hazards, the sporadic occurrence and highly localized effects of hail pose a particular challenge to hazard quantification, which forms the basis for any risk modeling. Such modeling helps the insurance sector to estimate the financial risks related to a hazard, as required, for example, by the Insurance Act 18 of 2017, and can guide measures to improve resilience.

Across the world, reliable records of hailfall including size information are limited to reports by volunteer observer networks (e.g., Held, 1974) and other sources, sometimes collected in databases of hail reports (e.g., Dotzek et al., 2009; Allen et al.,

https://doi.org/10.5194/nhess-2021-342
Preprint. Discussion started: 25 November 2021


Natural Hazards and Earth System Sciences Discussions

2015) or hailpad-equipped networks (e.g., Palencia et al., 2009). Leigh and Kuhnel (2001) were able to construct a regional risk model based on such reports and loss data alone.

For South Africa, Admirat et al. (1985) evaluated hailpad and hail reporting postcard data to quantify hailstorm properties in an area of 2800 km^2 in the “Transvaal Highveld," nowadays a part of the Gauteng region. In this domain, Smith et al. (1998) found on average 68.5 hail days per year in this area, much more than in other regions of similar size such as, for example, northern Italy, which is the highest hail-exposed region in Europe (e.g., Giaiotti et al., 2003). Of these, 3.3 days had hail greater than 31 mm. Grieser and Hill (2019) focus on hailpad derived metrics for hazard analysis and risk modeling. Since hailpad data sets either do not cover large enough areas or do not offer continuous observation in space and time, they are insufficient when considering the risk for portfolios spread over large regions or countries and affected by long-lived storm systems.

While distinction of hail from rain is often challenging, remote sensing data from either radar or satellite instruments is required to determine the spatial extent of hail events and to depict the geographic distribution of the hazard (Punge and Kunz, 2016). Alternatively, numerical modeling can be used to identify atmospheric conditions favorable for hailstorm formation (Kunz et al., 2020). In that case, climatologies over long time series can be generated (Dyson et al., 2020; Prein and Holland, 2018). These are however generally limited by model resolution and the inaccurate representation of convective initiation, since hailstorm formation is often related to local and meso-scale processes related to, for example, orographic lifting and mountain winds, low-level convergence zones, or land use inhomogeneities (Allen et al., 2020). Ground-based radar indicators of hail have been used for climatology (Cintineo et al., 2012; Junghänel et al., 2016; Fluck et al., 2021) and risk modeling (Puskeiler et al., 2016; Nisi et al., 2018; Schmidberger, 2018), but are often limited to country scales due to availability and inter-radar calibration issues. In South Africa, the use of radar data for nowcasting of hail has been studied for the Highveld (Ayob, 2019).

Even though satellite data provides a less accurate proxy for hail compared to radar, its big advantage is that the systems cover comparatively larger domains. The detection of hail via scattering of upwelling Earth-emitted microwave radiation is currently limited to satellites in low-earth orbit (Mroz et al., 2017; Ni et al., 2017; Bang and Cecil, 2019). Such data can be exploited for global analysis of hail occurrence as well as identification of atmospheric conditions for individual hailstorms, but they lack the temporal coverage required to examine the evolution of hailstorms. In contrast, indirect indicators have been designed to extract severe weather and hail signals from much more frequent and spatially detailed geostationary satellite imagery (Bedka et al., 2010; Melcón et al., 2016). An overshooting cloud top (OT) indicates an intense updraft capable of generating hail that can be detected in both visible and infrared data (Bedka and Khlopenkov, 2016; Khlopenkov et al., 2021). In particular, the most severe hailstorms show a clear OT signature (e.g., Kunz et al., 2018; Wilhelm et al., 2021), which makes OT detection an appropriate proxy to assess individual hail-producing cells and large-scale hail outbreaks that cause by far the largest part of the damage registered by insurers, and which can induce solvency issues when the risk was not properly estimated.

Punge et al. (2014, 2017) use the OT approach to develop a hail event dataset for Europe that served as the physical basis for the Willis European Hail Model, the first fully randomized stochastic hail model to cover all of Europe. Since 2014, the model has been established as a standard tool in hail risk estimation and pricing among insurance and reinsurance companies in Europe. A similar approach was later on applied to Australia (Bedka et al., 2018), but assessments of this kind are absent

https://doi.org/10.5194/nhess-2021-342
Preprint. Discussion started: 25 November 2021


Natural Hazards and Earth System Sciences Discussions

in many emerging markets around the world. Of these, South Africa is a prime example where hail is a common hazard. Therefore, we focus on South Africa in this article, refining the methodology to describe hail events more accurately. In contrast to Bedka et al. (2010), the Khlopenkov et al. (2021) OT detection technique provides a gridded probabilistic representation of an OT rather than a list of OT centroid pixel locations, accounting for both size and reliability of the updraft detections. The event definition procedure now tracks storm signatures over time, allowing to follow convective activity more closely. In the stochastic component of the model, rather than simply re-sampling historic events to describe possible future hazard, distributions for relevant event properties are modeled and sampled separately, conserving correlation among these properties. Improvements compared to the European and Australian hail models concern event definition, event parameter distributions, and detail of the stochastically generated footprints.

Sect. 2 presents the methodology and data sets used as input to the model, whereas Sect. 3 describes the derived hazard distribution and event sets. Then, event sampling and hail footprint generation are discussed in Sect. 4.

2 Methods and Data

2.1 Overshooting Top Detection

Intense thunderstorms are routinely observed from space in visible and infrared imagery from geostationary satellites for forecasting and warning purposes (Zinner et al., 2013; de Coning et al., 2015). In particular, in the infrared, high-reaching convective cloud tops atop updrafts appear as cold spots growing near to or above the tropopause level, surrounded by a warmer anvil (Adler et al., 1985). Cloudy air masses are propelled upwards in the storm's core before rebounding or dissolving again on a time scale of a few minutes.

Detection of these OTs has been automated by Bedka et al. (2010), revealing the climatological distribution in North America as well as in Europe (Bedka, 2011) and Australia (Bedka et al., 2018). An advanced version of the OT detection algorithm described by Khlopenkov et al. (2021) delivers a 3-km gridded probabilistic estimate of OT likelihood based on a statistical combination of tropopause-relative IR brightness temperature, prominence of an OT relative to the surrounding anvil, and the area and spatial uniformity of the anvil cloud surrounding an OT candidate region. The method was validated by Khlopenkov et al. (2021) using human OT identifications, as well as by Cooney et al. (2021) using OT identifications from gridded weather radar observations over the US. This method was found to perform much better than the Bedka et al. (2010) version used in previous climatology studies. False OT detections in very cold outflow near to actual OT regions is the most common source of error, though Sandmæl et al. (2019) showed that agreement between OT detections and severe weather conditions can be further improved using a combination of IR and visible wavelength signals.

A relation between hail size and OT intensity has been suggested in several studies (e.g., Bedka, 2011). Figure 2 illustrates how specifically the temperature difference between the coldest OT pixel and its surrounding anvil is related to the maximum expected size of hail (MESH) estimated by radar over the US (Murillo and Homeyer, 2019). No comparable analysis could be carried out for South Africa as a sufficient number of high-quality proximity radar scans or hail reports was not available, but it is physically highly plausible that a similar relation would be found.

https://doi.org/10.5194/nhess-2021-342
Preprint. Discussion started: 25 November 2021

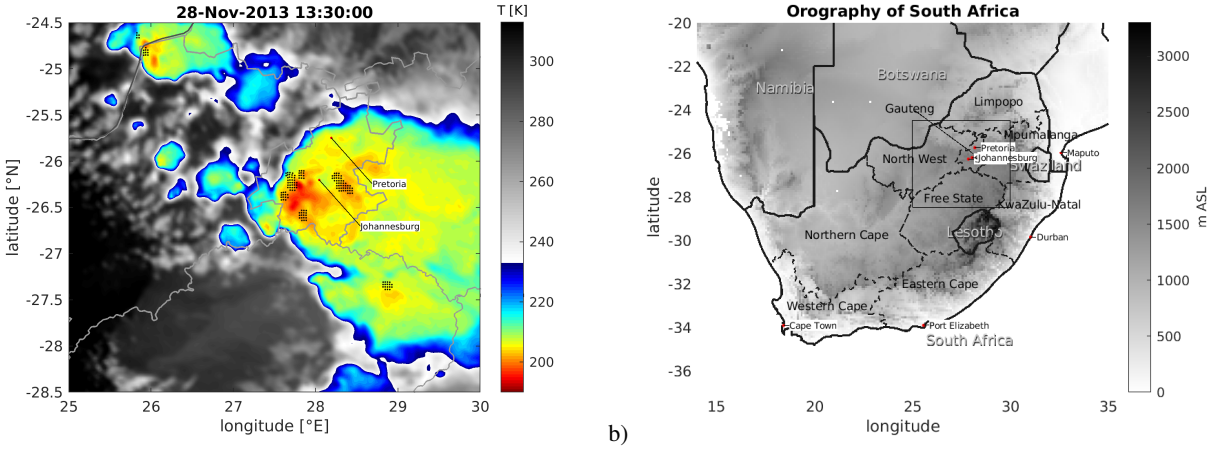

Figure 1. a) Meteosat IR image showing convective storm activity on November 28, 2013 at 1330 UTC. Colors represent $10.8\mu m$ channel brightness temperature and dots indicating detected overshooting tops (OTs, black) for this image. b) Map showing the relief of South Africa from SRTM (Farr et al., 2007), provinces and major cities.

Imagery of the Meteosat Second Generation (MSG) SEVIRI instrument (Schmetz et al., 2002) between January 2005 and December 2018 is scanned for potential hailstorms at a temporal resolution of 15 minutes. Since South Africa is not continuously covered by the high resolution visible imagery product of MSG, only the IR channel data (given as 10.8-μm brightness temperature) is provided to the detection algorithm. An example is shown in Fig. 1a, where brightness temperature during one of a very strong hail event on 28 November 2013 and detected OTs are displayed. Based on past experience, only OTs detected with a probability >50% and with a surrounding anvil cloud (green and yellow colors in Fig. 1a; the IR anvil detection index, a rating based on an anvil detection model accounting for viewing situations, greater than 10; see also Scarino et al., 2020) are used in this work. Their spatial distribution is depicted in Fig. 3. Clearly, convective storms are most common in the east of South Africa, along the Great Escarpment, including the south-eastern flanks of the Drakensberg and stretching north through the Mpumalanga province, where the terrain induces uplift to serve as a trigger for convective initiation. OT frequency decreases towards the west and towards the coast of the Indian Ocean.

Compared to Dyson et al. (2020), we note the absence of an OT frequency maximum over the country of Lesotho, even in the unfiltered OT data, and higher values to the north and southeast. We attribute this to the coarse spatial resolution of the ERA-INTERIM reanalysis used in that study, that is likely insufficient to resolve local orography. The high altitudes in southern Lesotho (mostly 2500–3500 m above sea level, cf. Fig.1b) seem to suppress deep convection to some degree, similar to the situation in the interior of the Alps in Europe (Punge and Kunz, 2016; Nisi et al., 2018).

2.2 Hail reports and insurance claims

Reports of hail observations are registered in continental-scale centralized databases for North America, Europe and Australia, including estimates of hail size. Such reports can play an important role for validating the severity of storms with detected

https://doi.org/10.5194/nhess-2021-342
Preprint. Discussion started: 25 November 2021

Natural Hazards and Earth System Sciences
Discussions

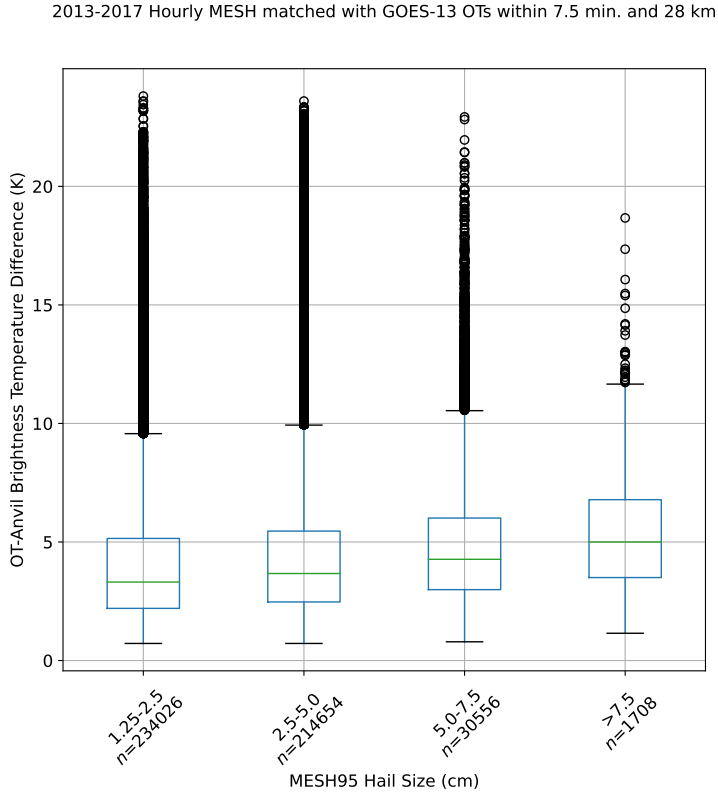

Figure 2. Maximum OT-anvil mean Brightness Temperature Difference (BTD) vs. hail severity categories based on radar-derived Maximum Estimated Size of Hail (MESH, Murillo and Homeyer, 2019) for 480 944 OTs detected over much of the continental US (115°–80°W, 30°–50°N) in the years 2013–2017, showing a clear correlation. Though GOES-13 has a slightly coarser spatial resolution (4 km at nadir) than MSG SEVIRI (3 km at nadir), the results shown here over this U.S. domain are believed to be representative of relationships for storms over South Africa.

OTs. As for South Africa no database of comparable extent is available. Reports in Europe and Australia (Bedka et al., 2018) have been used to estimate the hail size spectrum of events, but these spectra do not tend to vary greatly among continents (cf. Prein and Holland, 2018). In total, 26 884 reports were obtained from the European Severe Weather Database (ESWD) for the period 2005–2019, and 3 764 from the Severe Storms Archive of Australia's Bureau of Meteorology in the period 1950–2019. Reporting policies meant that events of hail diameter of 20 mm or more are covered, but in some cases reports with smaller stones accumulating to thick layers are included. A uniformly distributed random number between -0.5 and 0.5 was added to each reported hail diameter to compensate for rounding in the hailstone measurement process and to obtain a smooth distribution.

In addition, 1 423 claims of hail damage between 1984 and 2017 including a reference to a location were obtained from several insurance companies of South Africa (see Fig. 4). Data did not include information on the size of hail, hour of occur-

https://doi.org/10.5194/nhess-2021-342
Preprint. Discussion started: 25 November 2021

Natural Hazards and Earth System Sciences
Discussions

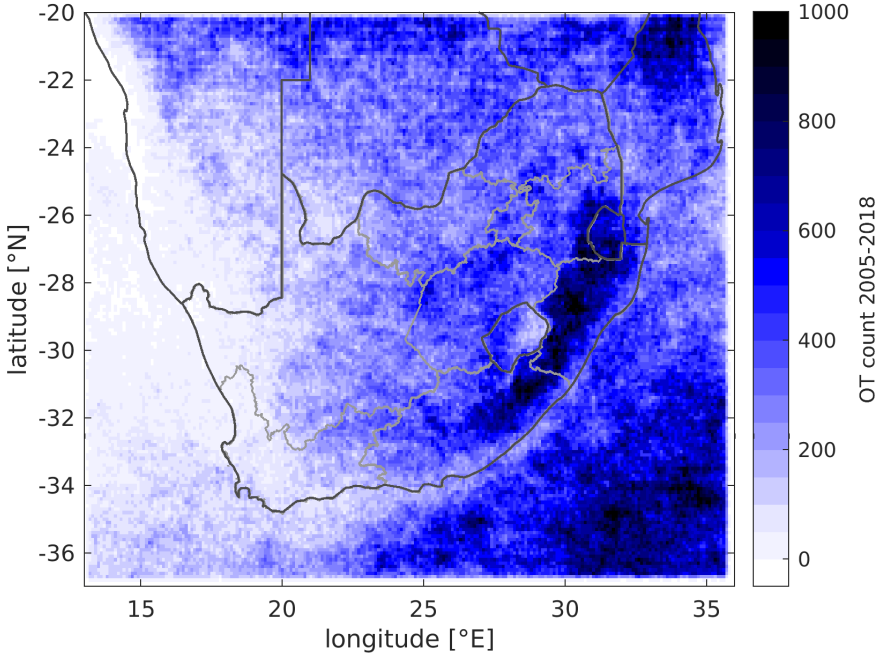

Figure 3. Distribution of 11 143 479 overshooting top pixels in the period 2005–2018 over South Africa and neighboring nations and seas.

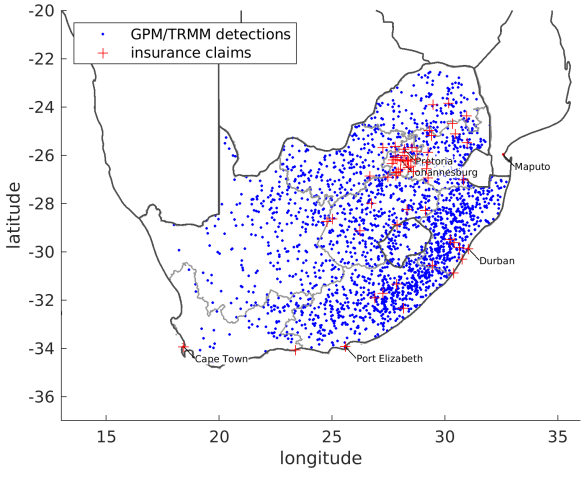

Figure 4. Claims locations of hail damage in South Africa (1984–2017) and passive microwave detections (1998–2018) in the model domain.

rence, or type of asset affected. Claims data tends to be biased towards population centers and – in this case – towards major hail days, but still has the advantage to provide direct evidence for hail occurrence.

https://doi.org/10.5194/nhess-2021-342
Preprint. Discussion started: 25 November 2021


Natural Hazards and Earth System Sciences Discussions

2.3 ERA-5 reanalysis data

ERA-5 (Hersbach et al., 2020) is the 5^{th} generation reanalysis of the European Centre for Medium-Range Weather Forecasting (ECMWF). It is a global observation-guided model representation of past weather. Data were obtained for the period 2005–2018 at a spatial resolution of 0.25°and hourly resolution. While CAPE and the height of the freezing level are provided as output variables, bulk wind difference between the near-surface (10 m) and 6 km above the ground (0–6 km wind difference) was computed based on pressure level data using linear interpolation.

2.4 Passive Microwave hail retrievals

Scattering of surface emitted microwave radiation by hailstones enables hailstorm detection by satellites (Cecil, 2009). This measurement principle has the advantage that in contrast to OTs, the signal is directly caused by hailstones, at the cost of spatial and temporal coverage, commonly limited to two overpasses per day, and at the risk of nonuniform beam filling (NUBF) of the field of view. Beam sizes of current generation sensors (e.g., Petty and Bennartz, 2017) are on the same order of magnitude as convective storm core diameters, meaning that sensor and storm need to be align for successful detection. In this work, such detections from TRMM and GPM satellites (Bang and Cecil, 2019, 2021) over the South African domain were evaluated for the period 1998–2019. Cases with a hail probability greater than 10% over South Africa and Lesotho were retained. Along with the damage claims, they are used to compare hail environments in South Africa to those in Europe and Australia (Punge and Kunz, 2016; Bedka et al., 2018).

2.5 OT filtering by conditions from reanalysis

The OT detection algorithm has been extensively calibrated and tested against severe weather reports and radar data (Bedka and Khlopenkov, 2016; Sandmæl et al., 2019; Cooney et al., 2021). Still, in some cases OT features may have been falsely detected or not have produced hail on the ground, for example, due to melting during fall through a deep column of warm air. Also, for hazard modeling purposes, the focus is on the identification of larger clusters of severe convective storm events likely to have produced hail in the event lifetime rather than detecting each isolated storm with enhanced hail potential. At first, a filter is applied to the OT data based on surrounding atmospheric conditions obtained from ERA-5, before clustering detections in space and time. Note that the purpose of this filter is distinct from other studies aiming to identify hail-prone conditions from reananlysis (e..g., Taszarek et al., 2020; Dowdy et al., 2020; Prein and Holland, 2018) that tend to suggest much stricter criteria.

For South Africa, the filter design used for Europe and Australia (Bedka et al., 2018) has been retained. For this work, conditions near OT detections are interpolated spatially from the much higher resolved ERA-5 reanalysis data set instead of ERA-INTERIM (25 km rather than 80 km). In contrast to ERA-INTERIM, ERA-5 has hourly rather than 6-hourly fields, so values at the full hour are used for OT detections in the following 60 minutes. This reduces false filtering due to the models failure to resolve, for example, the rapidly evolving CAPE field that has a strong diurnal cycle. Bulk wind difference from surface to 6 km and freezing level for microwave hail detections and insurance claims and in the vicinity of OT detections in South Africa and Lesotho are shown in Fig. 5. OTs occur at somewhat lower 0–6 km wind difference and greater freezing

https://doi.org/10.5194/nhess-2021-342
Preprint. Discussion started: 25 November 2021


Natural Hazards and Earth System Sciences Discussions

level compared to microwave detections, confirming the filter choice in Punge et al. (2017). Note that microwave hail and OT detections occur most frequently at a 0–6 km wind difference between 10 and 20 ms^{-1}, and a higher threshold would exclude a relevant fraction of situations where hail is likely based on the microwave algorithm. Damage reports often occur at 0–6 km wind difference between 20 and 30 ms^{-1}, indicating a bias towards the more organized storms producing more damaging hail. But given the high concentration of these claims in populated regions, we refrain from using a more restrictive thresholds based on this data alone. As 9.5% of the OTs occur at a melting level of less than 2 400 m, but ony 3.5% of the microwave hail detections and and 2.5% of the claims, a lower threshold of 2 400 m was introduced for this parameter.

OTs are thus retained if the surroundings of a given OT fulfill minimum conditions of convective instability (>100 Jkg^{-1}), 0–6 km wind difference (>1.5 ms^{-1}) and the height of the melting level (>2 400 m, <4 845 m above the ground). The spatial distribution of the filtered OTs is shown in Fig. 6. It is found that the filter removes OT detections in particular over the ocean, central Moçambique and the Lesotho Highlands (cf. 3). The latter feature is due to the minimum freezing level condition and remains to be confirmed by independent observations.

Regarding the hail signals over the south-western Indian Ocean, along the south eastern coast of South Africa, these are also present in Prein and Holland (2018, , Fig. 11), as well as in passive microwave data (Bang and Cecil, 2019, Fig. 7).

A final judgment on the actual occurrence of significant hail on the ground will require surface observation data that is difficult to obtain. Similarly, little is known about the likelihood of hail closer to the tropics, as ground reports are rare and numerical schemes to compute hail probability such as those used by Dyson et al. (2020) are usually developed and tested in mid-latitude or sub-tropical settings.

2.6 Event definition: Grouping hail activity

Figure 7 illustrates the definition of historic events based on observed OT data. These events are formed by computing the spatial and temporal distance between OT detections. OTs are assigned to the same event if they are separated by less than 1 hour and less than 30 km. This simple approach can detect both single cells and other more organized forms of convection including squall lines. Event centroids are defined as the mean latitude and longitude of the event OTs. The event is approximated by an ellipse and characterized by its length, width, orientation relative to the meridian, as well as the fraction filled with OTs and the highest OT-anvil mean temperature difference among event OTs as a criterion for storm severity (cf. Fig. 2). Lifetime and propagation speed are estimated based on the initial and final OT occurrences within the event. Events can overlap when several storms pass over the same region on a given day.

The event definition criteria are more restrictive compared to Punge et al. (2014), so the events are better constrained to zones of possible hail activity. Events made up by OT detections only at a single time step, hence lasting for less than 30 minutes, are neglected. In total, 33 820 events were found.

The duration and propagation speed of severe convective storms events – both not considered in Punge et al. (2014) – are given in Fig. 8a and b). The distribution of durations is exponential in shape, in line with radar-based studies (Schmidberger, 2018; Fluck et al., 2021). While duration is roughly proportional to length, it becomes clear that propagation speed varies over a wide range. Most frequently, the speed ranges around 30–35 kmh^{-1} (≈8–10 ms^{-1}), slightly lower than the range of 10–30 kt

https://doi.org/10.5194/nhess-2021-342
Preprint. Discussion started: 25 November 2021

Natural Hazards and Earth System Sciences
Discussions
Open Access
EGU

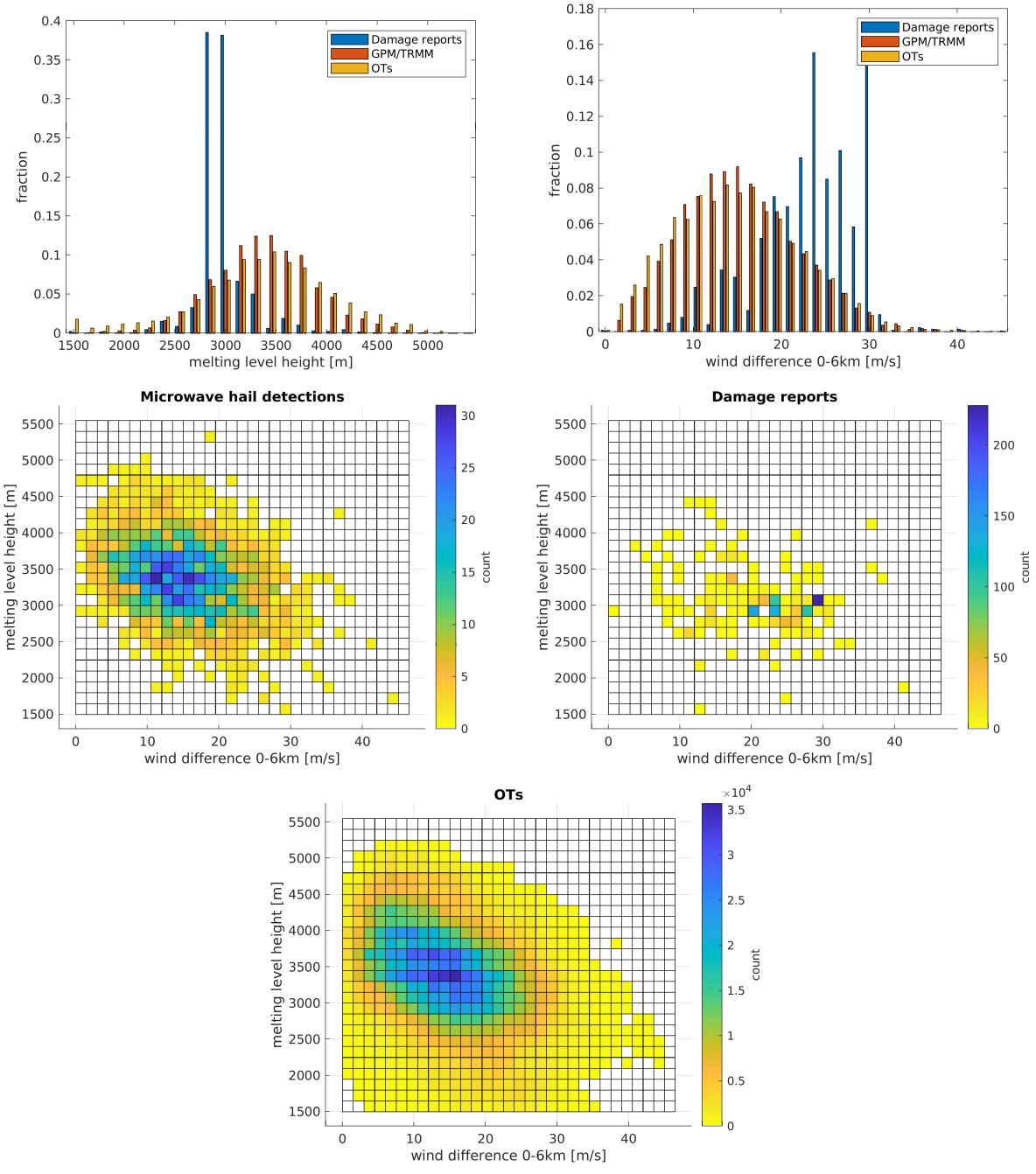

Figure 5. Distribution of ERA-5 0–6 km wind difference and melting level height in hail claims(1984–2017), passive microwave detections(1998–2019), and OTs (2005–2018). Top row: probability distribution; Bottom row: bi-variate histogram for 0–6 km wind difference and freezing level. Only situations with positive CAPE in ERA-5 were used for these computations.

https://doi.org/10.5194/nhess-2021-342
Preprint. Discussion started: 25 November 2021

Natural Hazards and Earth System Sciences
Discussions

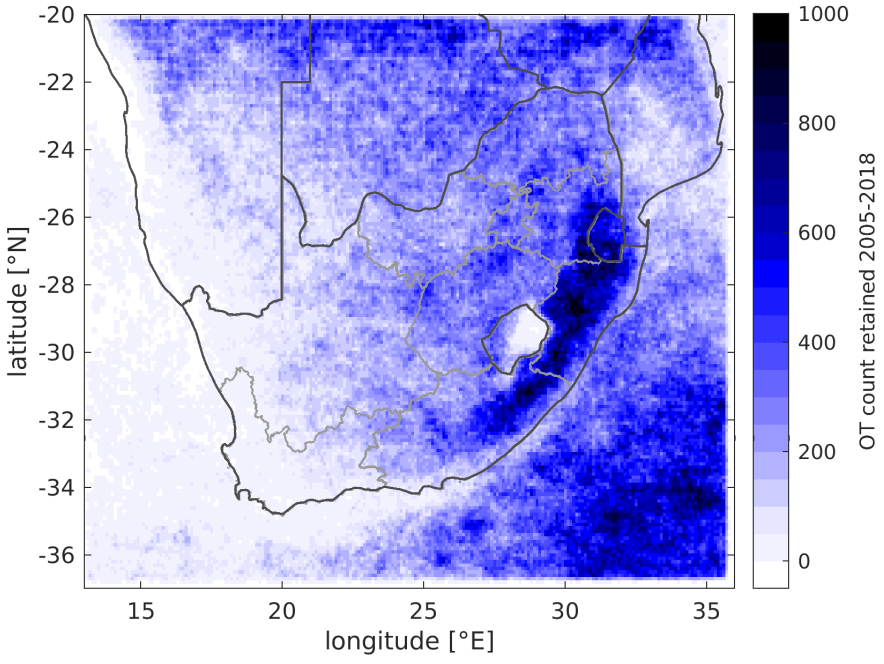

Figure 6. Map of 8 272 509 overshooting top pixels retained by the filtering for atmospheric conditions.

($\approx$ 18–55 $\mathrm{km\,h^{-1}}$) found by Carte (1966). Very high values beyond 100 $\mathrm{km\,h^{-1}}$ are explained by cases where convection is triggered simultaneously over a larger domain and OTs from several storms are unintendedly grouped to an event.

3 Hazard distribution and event properties

In this section, we describe the spatial distribution of potential hail events for the model as well as additional event properties. Distribution functions are used to approximate the historic event set computed in the previous section, complemented with hail size information from reporting. Stochastic events are generated using these distribution functions for relevant event properties, and 14-year samples from the stochastic event set are compared to the historic data. The full stochastic event set covers 25 000 years with a total of 21 093 957 events spanning 3 442 346 days. The key challenge in generating this event set is to ensure conservation of event properties and their inter-relationships. It is addressed by drawing from historic distributions using correlated random numbers where required.

The spatial event distribution is obtained by normalizing the annual OT frequency, counted on a rectangular 0.3° $\times$ 0.5° (lat/lon) grid with the average number of OTs per event (Fig. 9). This grid was chosen to retain spatial details of OT occurrence due to physical processes, but dampen local accumulation of OTs on individual pixels caused by the accidental passage of

https://doi.org/10.5194/nhess-2021-342
Preprint. Discussion started: 25 November 2021

Natural Hazards and Earth System Sciences
Discussions

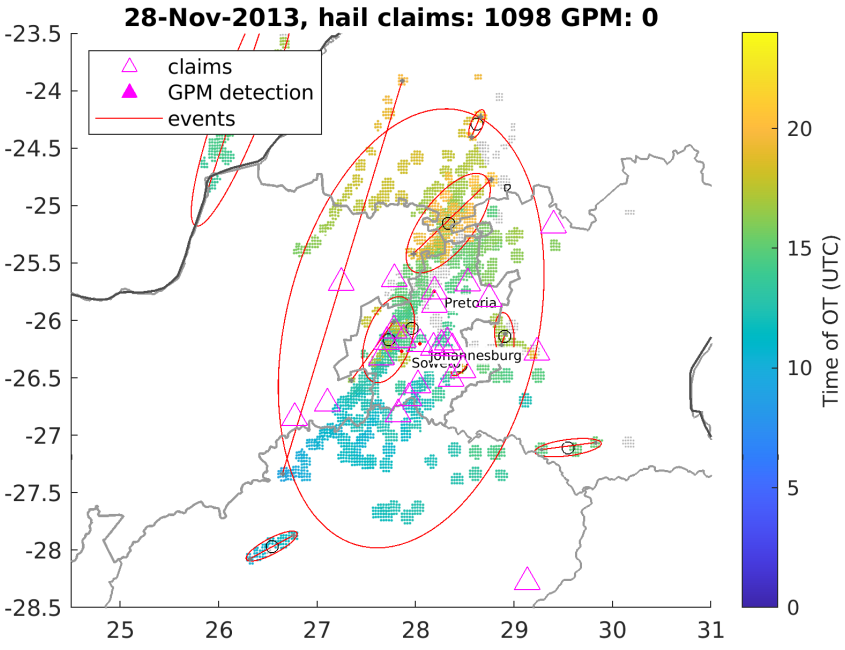

Figure 7. Convective storm activity in the Gauteng region of South Africa on November 28, 2013. Filtered OTs (gray dots), retained OTs (color-coded by time), hail claims (pink) and event definition (ellipses). A line connects the locations of the initial and final OT locations, determining the orientation of the ellipse. Two smaller events overlap the main event centered over the Gauteng region, as the associated cells developed at a later time, separately from the main activity.

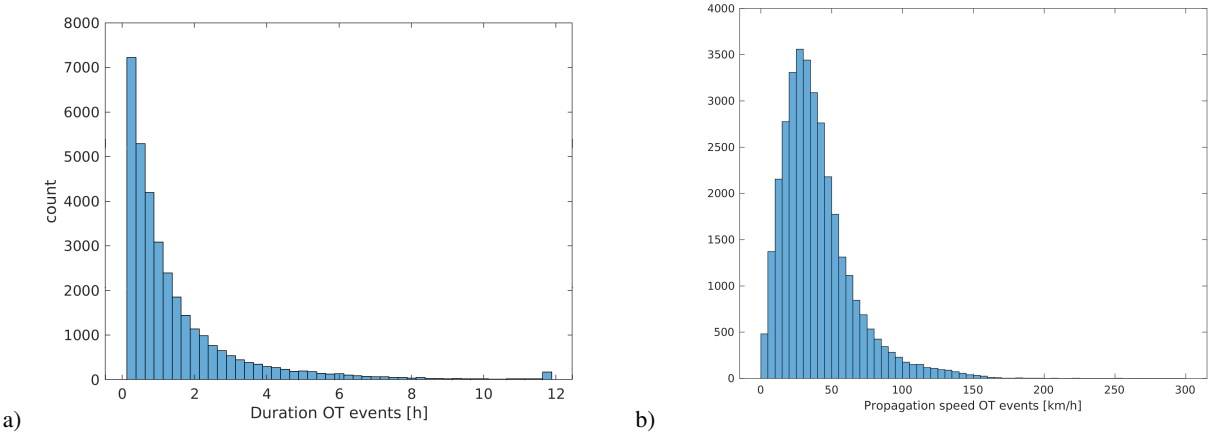

Figure 8. Histogram of hail-filtered OT event a) duration and b) propagation speed, 2005–2018.

https://doi.org/10.5194/nhess-2021-342
Preprint. Discussion started: 25 November 2021

Natural Hazards and Earth System Sciences
Discussions

Table 1. Hail event property distributions and parameters

variable	distribution	shape parameter	scale parameter	location parameter
length l [km]	GEV	0.57	26.68	37.33
width l [km]	GEV	0.90	7.92	13.00
event-to-storm area ratio $1/f$	GEV	0.20	1.26	2.36
hail size d [cm]	Gamma	3.70	0.83	

multiple storms in the same location. The implicit assumption with this method that events are distributed in the same manner as OTs implies a certain amount of additional smoothing that can be neglected at scales larger than the event length.

Following Punge et al. (2014), both annual and daily cycles are modeled with Gaussian distributions. For the day of year, domains of $3° \times 5°$ are considered, and depending on the number of events, either a mixture of two Gaussians – to accomodate for two peaks in spring and autumn – or a simple Gaussian distribution (summer peak) is fitted. The relatively large grid was chosen to ensure a stable solution when fitting this complex function, also in regions with few OTs. For each batch of stochastic events representing 250 years, the following procedure is applied: Days are drawn from the boxes distribution for the N events in this box and the 8 surrounding boxes. To mimic the grouping of events in severe days, the same day is then attributed to blocks of $N^{1/3}$. Finally, the day is retained only for N/9 events at random. This procedure has been found empirically to approximate the observed space-time distribution of days in a satisfactory manner.

In a similar way, the hour of day is determined. On the same $5° \times 3°$ grid, the distribution is determined. Then times are drawn from this distribution for the N events from a region of $10° \times 6°$ around the boxes center and retained with a chance of 1/4. Again, the box dimensions may appear arbitrary, but have been carefully chosen to capture observed spatio-temporal variability.

Figure 10 shows the daily and seasonal variation of the observed (a) and modelled (b, same duration – first 14 years) events. There is a clear maximum in austral summer (December and January, also cf. Fig. 11a). Also note the secondary maximum in fall (around days 100–150, i.e. April and May) during nighttime, represented in the model. For the Highveld region, Smith et al. (1998) report a somewhat earlier maximum in November and December. Indeed we find the convective season peaks around this time in the Highveld and KwaZulu-Natal, and in the first half of November over the Gauteng (not shown). It is shifted towards fall over the Southern Ocean. Peak time of day is between 14:00 to 15:00 UTC, or 4–5 pm South African Standard Time, slightly earlier than Smith et al. (1998, 5–6 pm) but consistent with Olivier (1990) (Fig. 11b). The daily cycle is most pronounced in summer. The temporal climatologies of historic (Fig. 10a) and modeled (Fig. 10b) events match rather well, with the model slightly overestimating events in the tails of the Gaussians. However, during such low activity periods, the OT algorithm may however miss some lower-topped storms that can still produce hail on the ground.

https://doi.org/10.5194/nhess-2021-342
Preprint. Discussion started: 25 November 2021

Natural Hazards and Earth System Sciences
Discussions

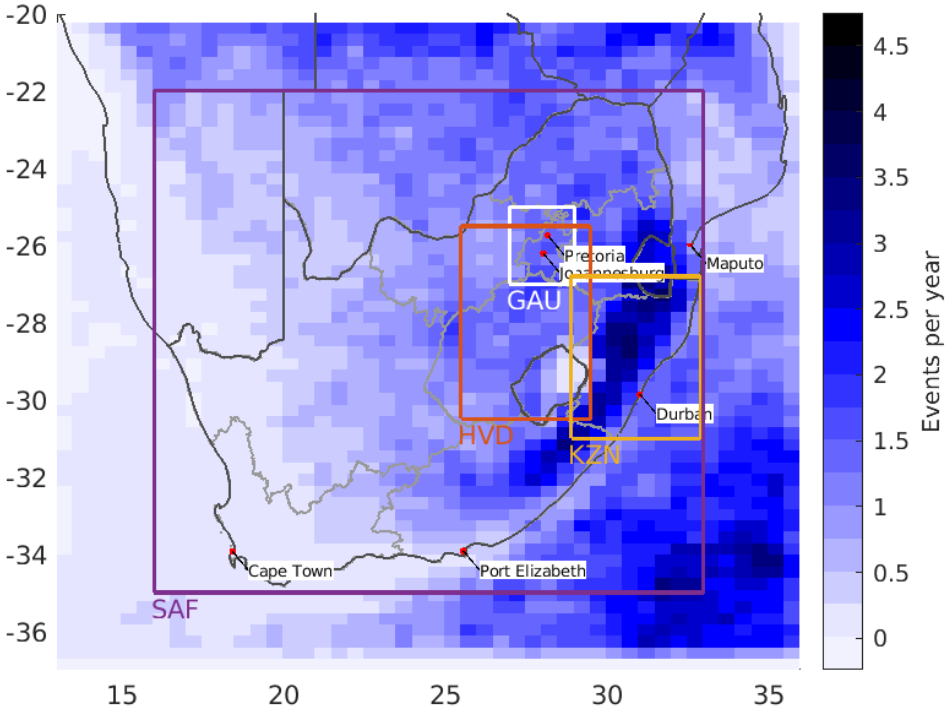

Figure 9. Event frequency distribution used for stochastic modeling. Boxes show regions discussed in Sect. 3.5.

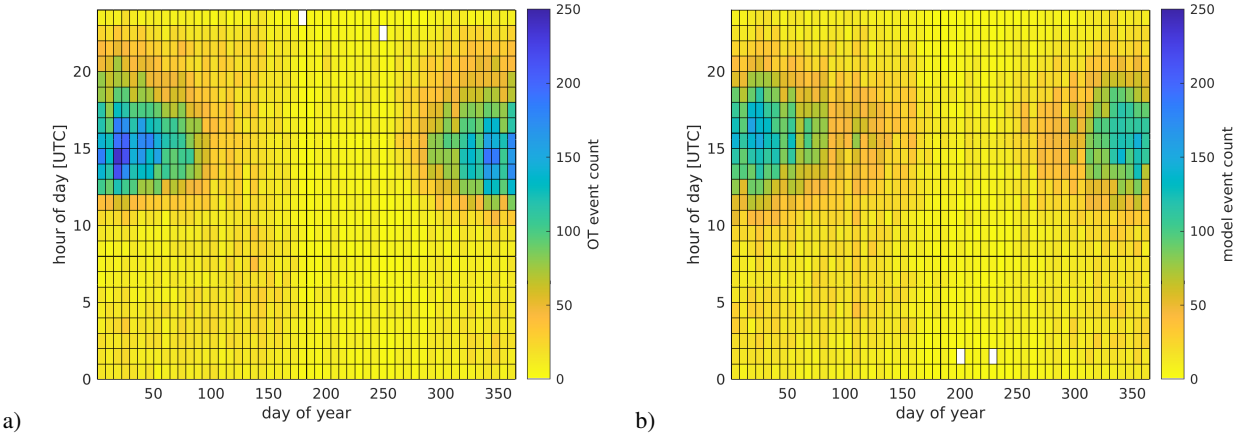

Figure 10. Distribution of events in time of day and day of year: a) historic events 2005–2018; b) stochastic model events.

https://doi.org/10.5194/nhess-2021-342
Preprint. Discussion started: 25 November 2021

Natural Hazards and Earth System Sciences
Discussions
Open Access
EGU

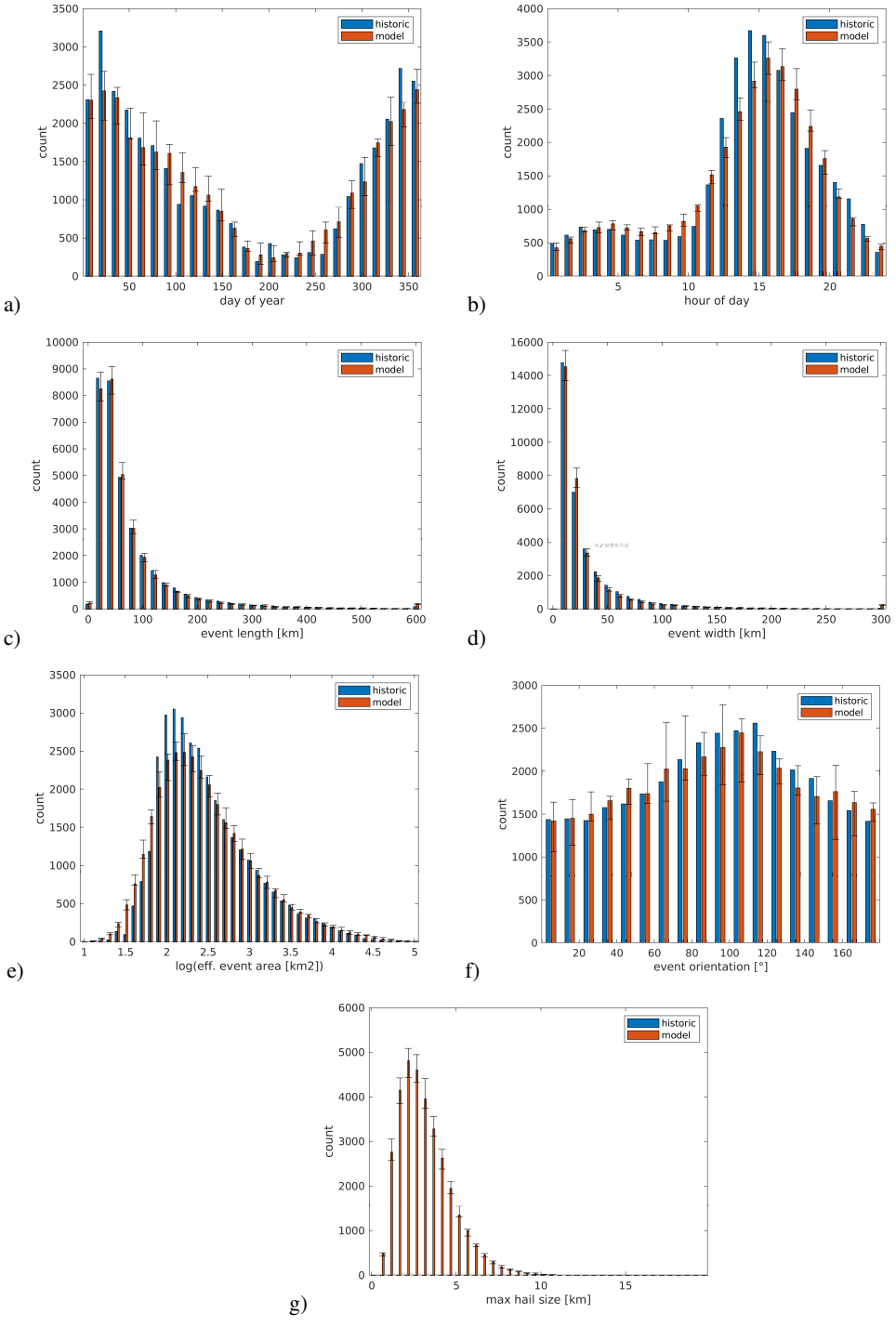

Figure 11. Distributions for properties of historic and stochastic events. With modeled events, (error) bars indicate the median (spread) among 7 independent samples of 14 years length. Hail sizes are unknown for the historic events, hence blue bars are missing in part g).

https://doi.org/10.5194/nhess-2021-342
Preprint. Discussion started: 25 November 2021

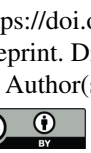

Natural Hazards and Earth System Sciences
Discussions

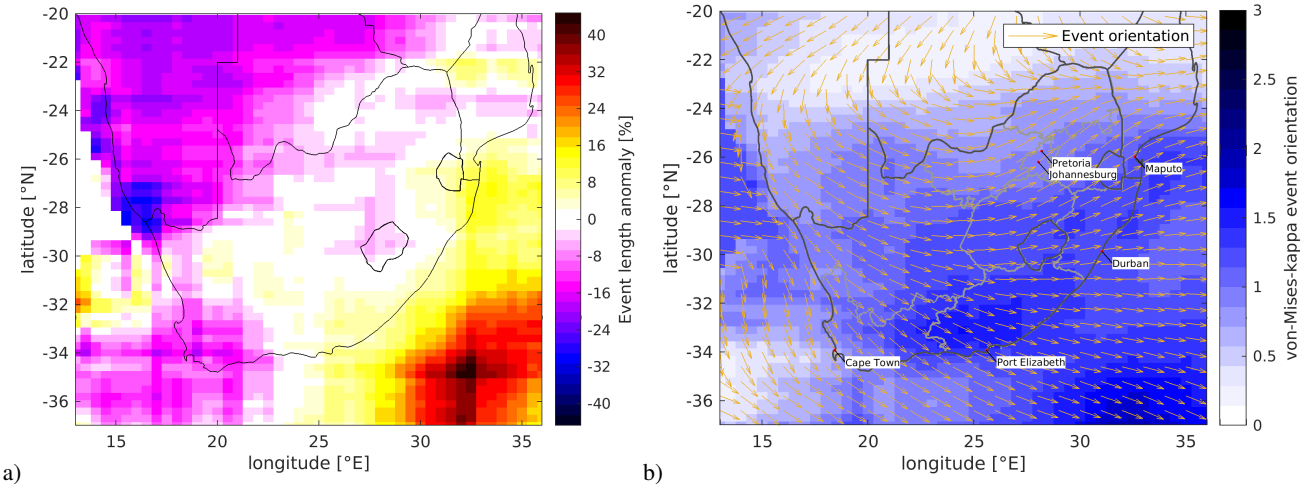

Figure 12. (a) Spatial variation of mean event length (%). (b) Spatial variation of event orientation, location parameter (arrows) and the shape parameter κ of the von-Mises distribution derived from the observed OT events.

3.1 Geometric event properties

Both event length l and width w distributions (Fig. 11c and d), determined from the observed OT events as described in Sect. 2.6, decay rapidly with increasing values. In contrast to previous model versions, we choose to approximate both properties with generalized extreme value (GEV) distributions rather than exponential distributions. This improves the fit in particular on the lower end.

The distributions are well approximated by the GEVs. As an exception, low width are somewhat over-represented, which can be attributed to the design of the event definition procedure for historic events. The GEV also tends to give unrealistic large values, which is why length and width have been truncated at 1.5 times the largest observed values, which corresponds approximately to the size of the entire country (1 445 km $\times$ 677 km).

In addition, the fraction f of the event area (the area of the ellipse spanned by major and minor axis of lengths l and w, $\pi/4\ l\ w$) covered by OTs/hail streaks is modeled. In this case, a GEV is fitted to the inverse of that fraction, the event-to-storm area ratio. This function was found to match observations well, as the inverse has no upper bound but very OT-sparse events are extremely rare. Fig. 11e) shows a histogram for the logarithm of the effective event area, i.e. the product $\pi/4\ l\ wf$. For the highest class ($> 10^5$ km^2), the fraction in the stochastic set is significantly higher, while the match is otherwise satisfactory. Table 1 lists the distributions and parameters for these event properties.

The orientation, or the direction of the major axis of an event, generally aligns with the direction of propagation. We find that most frequently, events have an orientation of around 100°, i.e., propagate eastward to southeastward (Fig. 11f).

Event properties can vary across the South Africa domain, so a box-window average over a 2.5 degree window is used to estimate these variations and scale properties in from the historic event set. Fig. 12a shows the spatial variation of event length

https://doi.org/10.5194/nhess-2021-342
Preprint. Discussion started: 25 November 2021


Natural Hazards and Earth System Sciences Discussions

in %, and Fig. 12b represents the most common orientation, obtained by fitting a von-Mises-distribution (Mardia and Zemroch, 1975) to the regional events. Events occurring offshore, where MCS are more common than over land (Feng et al., 2021), tend to run longer, whereas events are shorter in the western part of the domain, hinting towards less organized forms of convection. Orientation varies from south-eastward in the south-west to north-eastward in the north-east and is most aligned over the Eastern Cape region. Garstang et al. (1987) found winds from the north-westerly sector prevail at 850 hPa on convective storm days in north-eastern South Africa, but from a much smaller sample. The greater spread in orientation towards the north and west can be explained by the prevalence of storm systems affecting larger regions at the same time, hence grouping multiple parallel storms, as well as by small, quasi-stationary events whose orientation does not reflect an influence of storm propagation.

3.2 Hail diameters

At present, the maximum hail diameter cannot be estimated accurately from geostationary satellite measurements alone. Marion et al. (2019) suggest that convective storm severity be linked to OT area. Khlopenkov et al. (2021) also show a relationship between hail size and the difference between OT temperature and the tropopause temperature. In this study, we assume that hailstone size is best approximated from the vertical extent of overshooting above the surrounding anvil, a proxy for the strength of the updraft supporting the hailstones during growth. Hence the temperature difference between the OT and the surrounding anvil is used as a proxy for hail size, as supported by Fig. 2, and the highest such temperature difference of all OTs within an event characterizes the event's severity.

The distribution of hail diameters in databases is usually truncated at the lower end. For example, ESWD has a lower limit of 2 cm unless the hail accumulates to a thick layer. However, crops can be severely damaged by hailstones as small as 0.7 cm (e.g., Changnon, 1971). Therefore such lower diameters are also represented in the model. Situations with crop damage due to large amounts of even smaller hailstones or graupel are not considered here, as their formation is not limited to severe convective storms.

In the stochastic model, we assume that the maximum hail diameters of the stochastic events follow the same distribution as large hail diameters recorded in the databases. Hail diameters for all hailswaths within an event are derived from the attributed largest hail diameter, and the hail sizes decrease from the center of the event. This means that hailswaths with small hail sizes are more common in the model than the distribution derived from the database of maximum diameters would suggest. That is also the case in reality, as hail with a small diameter is less likely to be recorded in a database than large hail. Indeed hailpad data suggests hail frequency increases exponentially with decreasing size (Sioutas et al., 2009; Berthet et al., 2011).

Hailstone density greatly impacts the fall speed and therefore the damage potential for such stones (Heymsfield et al., 2014), but in practice little is known on its distribution, and hence this factor is not considered, and damage functions are derived from the maximum hail diameter alone.

3.3 Length-severity correlation

An important feature of the hail model is that it conserves the statistical correlation of event properties. The most relevant properties that are correlated are event length, event width, event maximum hailstone size, and fraction of event area covered

https://doi.org/10.5194/nhess-2021-342
Preprint. Discussion started: 25 November 2021

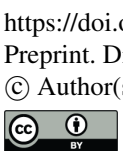

Natural Hazards and Earth System Sciences
Discussions

by hail streaks. The scatter plot of length and width (Fig. 13a) confirms that correlations between these event properties are

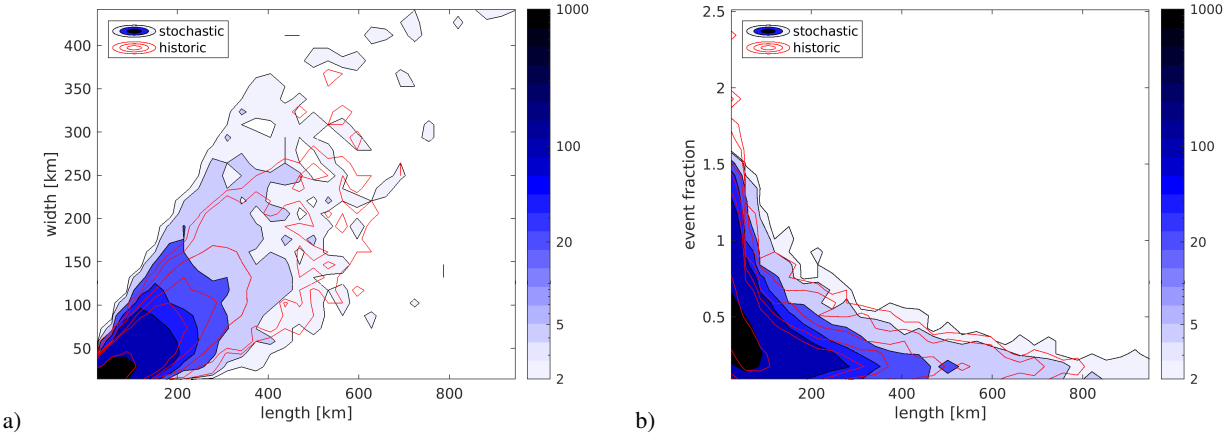

a) b)

Figure 13. Scatter plot of correlated historic and stochastic event properties: a) length and width, b) length and fraction of event covered by hail.

conserved in the model. As in Punge et al. (2014), the correlations between length and width to storm severity – represented by minimum OT temperature difference for historic events – are likewise conserved here. By the same method, the fraction of the event area affected by hail ('effective track area') was also taken into account. This is achieved by first drawing correlated sets of random numbers for each property from a uniform distribution and determine ranks. Then, for each property, we draw values from the actual distribution, sort them, and attribute to events using the pre-determined ranks.

Figure 13b shows the relation of event fraction and length, indicating that in large events, a lower fraction of the area is affected. Table 2 summarizes the Spearman rank correlations of the four variables considered. Longer hail events thus tend to be wider, have larger maximum hail diameter, and a lower fraction of the event area covered by hail streaks.

Table 2. Spearman rank correlation matrix of OT event properties.

property	set	length	width	maximum hail size	event-to-storm area ratio
length	historic	1.00	0.89	0.39	0.75
	model	1.00	0.90	0.39	0.49
width	historic	0.89	1.00	0.41	0.61
	model	0.90	1.00	0.40	0.43
severity	historic	0.39	0.41	1.00	0.17
	model	0.39	0.40	1.00	0.16
event-to-storm area ratio	historic	0.75	0.61	0.17	1.00
	model	0.49	0.43	0.16	1.00

https://doi.org/10.5194/nhess-2021-342
Preprint. Discussion started: 25 November 2021

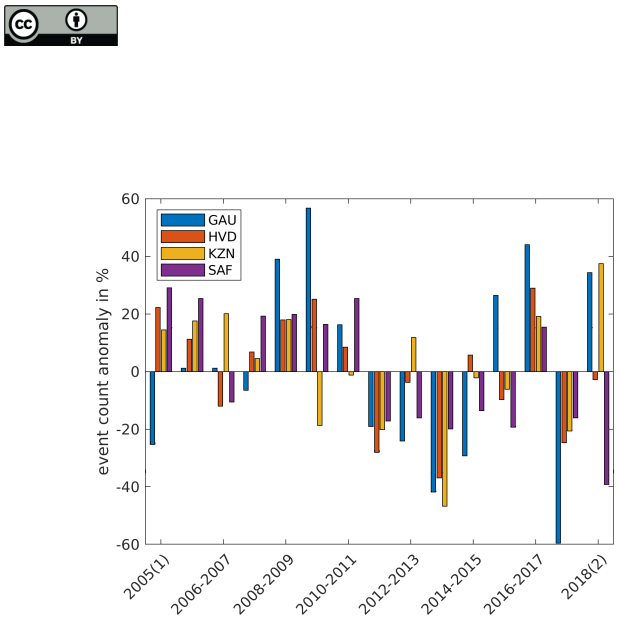

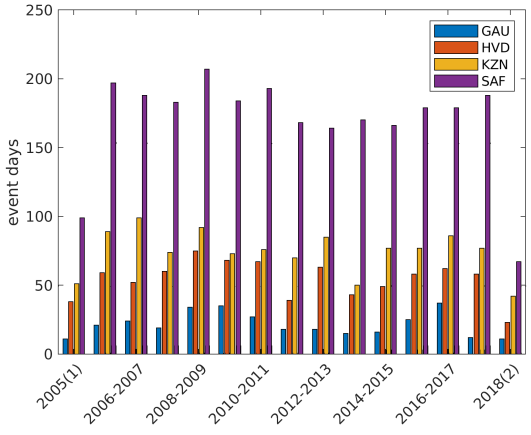

Figure 14. Time series of event count anomaly (deviation of the annual sum from the 14-year mean, left) and event days (right) per year (July–June) for regions Gauteng (GAU, regional annual mean event count 35), Highveld (HVD, 152), KwaZulu-Natal (KZN, 181) and South Africa (SAF, 1259). The July–June period is considered more appropriate as the Austral summer season is not split among years. For the 2004/2005 period, only events in 2005 are covered; likewise 2018/2019 covers only the last 6 months of 2018. When computing the event count anomalies for these years, the overall repartition of events to half years was taken into account.

3.4 Inter-annual variability

The time series in Fig. 14 shows considerable year-to-year variation in the annual number of hail events and hail days. As could be expected, smaller regions show relatively higher variability, but there is strong correlation between the two. This information can be helpful to understand the year to year variation of hail hazard and resulting losses. Note, however, that the year 2013/2014 had the second-lowest event count in the Gauteng region, despite the large damage from the November 28 event. Figure 15 shows patterns for the first five years of the historic event set (left), along with five years of the stochastic event set for a visual impression of spatio-temporal variability. The model has fewer events in the north compared to the observed event count as it is based on the scaled OT frequency instead of events, and events in this region contain fewer OTs. The modeled distribution appears overly smoothed at lower rates, but this is unlikely to be a concern.

3.5 Intra-annual variability

Quite relevant in practice is the representation of multiple events occurring on a single day, not considered by Punge et al. (2014). In fact, it turns out that only 15 % of the event days have just one event, whereas on a few occasions, more than 30 events were detected on a single day. Figure 16 shows the number of days with a given number of observed events per day for the South Africa domain (SAF, for simplicity defined as the area between -35 and -22° N, 16 and 33° E) and several sub-regions (see Fig. 9). Specifically, the Highveld (HVD) and KwaZulu-Natal (KZN) as the most populated and most storm-affected regions and the Gauteng (GAU) as the largest connected urban area with a significant concentration of assets were

https://doi.org/10.5194/nhess-2021-342
Preprint. Discussion started: 25 November 2021

Natural Hazards and Earth System Sciences
Discussions

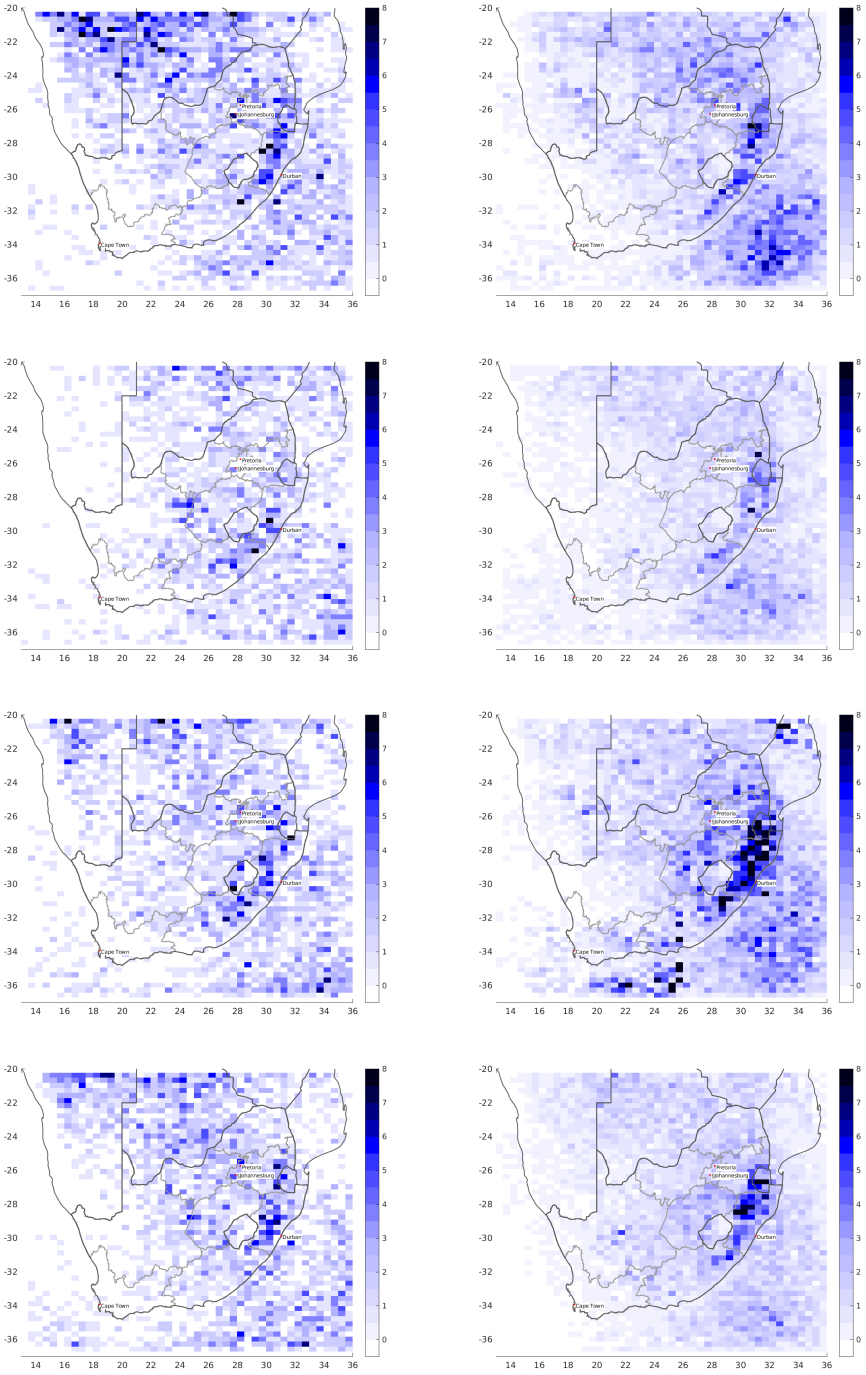

Figure 15. Spatial patterns of annual event distribution for years 2005/06 to 2008/09 (left) and in the stochastic event set (right).

https://doi.org/10.5194/nhess-2021-342
Preprint. Discussion started: 25 November 2021

Natural Hazards and Earth System Sciences
Discussions

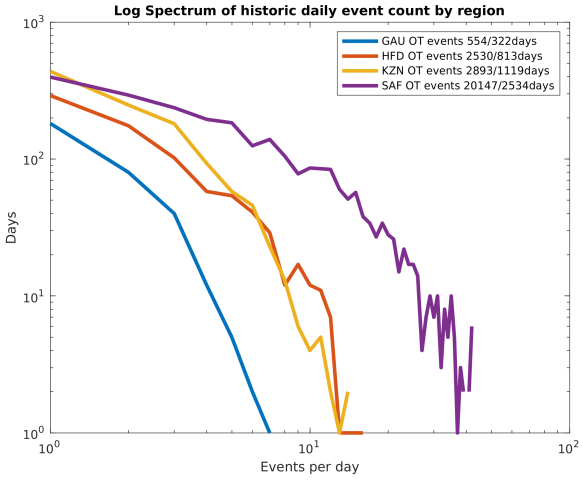

Figure 16. Spectrum of number of events per day on historic event days for regions SAF (entire country), HVD (Highveld), KZN (KwaZuluNatal) and GAU (Gauteng).

considered. Naturally, the smaller the domain, the lower the respective counts. Over the Highveld, the events are concentrated on a smaller number of days compared to the similar-sized KZN region.

The panels in Fig. 17 show the same regional frequency spectra, comparing the historic OT events to 6 equivalent subsets of the stochastic set. For example, the Highveld region has 2 075 hail events over 700 days (or around 150 hail events and 50 hail days per year), while in an equivalent sample of subsets from the stochastic event set, the event count ranges from 1 883 to 2 162 events on 671 to 703 days. The result is satisfactory for the South Africa and Highveld regions, whereas for KwaZulu-Natal events concentrate on slightly fewer days. Given the absence of multiple-event treatment in previous model versions, this will enable improvement for the estimation of damage on individual days.

In the Highveld region, there were 74 days per year with OT detections, 58 with OT events and 62 in the stochastic event set. These numbers were 96, 80, 71 for KwaZulu-Natal and 32, 23, 28 for the Gauteng region, respectively. In contrast, Smith et al. (1998) found 69 hail days per year from hail reporting from a network of voluntary observers by mail, for a portion of the Gauteng (2 800 km^2). However, severe hail (>31 mm in diameter) was found on 3.3 days per year on average. When considering only hail of this size, the stochastic event set has 14.5 hail days per year in the Gauteng region.

4 Event footprints

4.1 Importance sampling

When applying the risk model to an insurer's portfolio, going through millions of events for – potentially – millions of assets is a time consuming process. While the complete event set is optimal for describing hail hazard, an intermediate step, importance

https://doi.org/10.5194/nhess-2021-342
Preprint. Discussion started: 25 November 2021

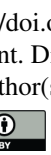

Natural Hazards and Earth System Sciences
Discussions

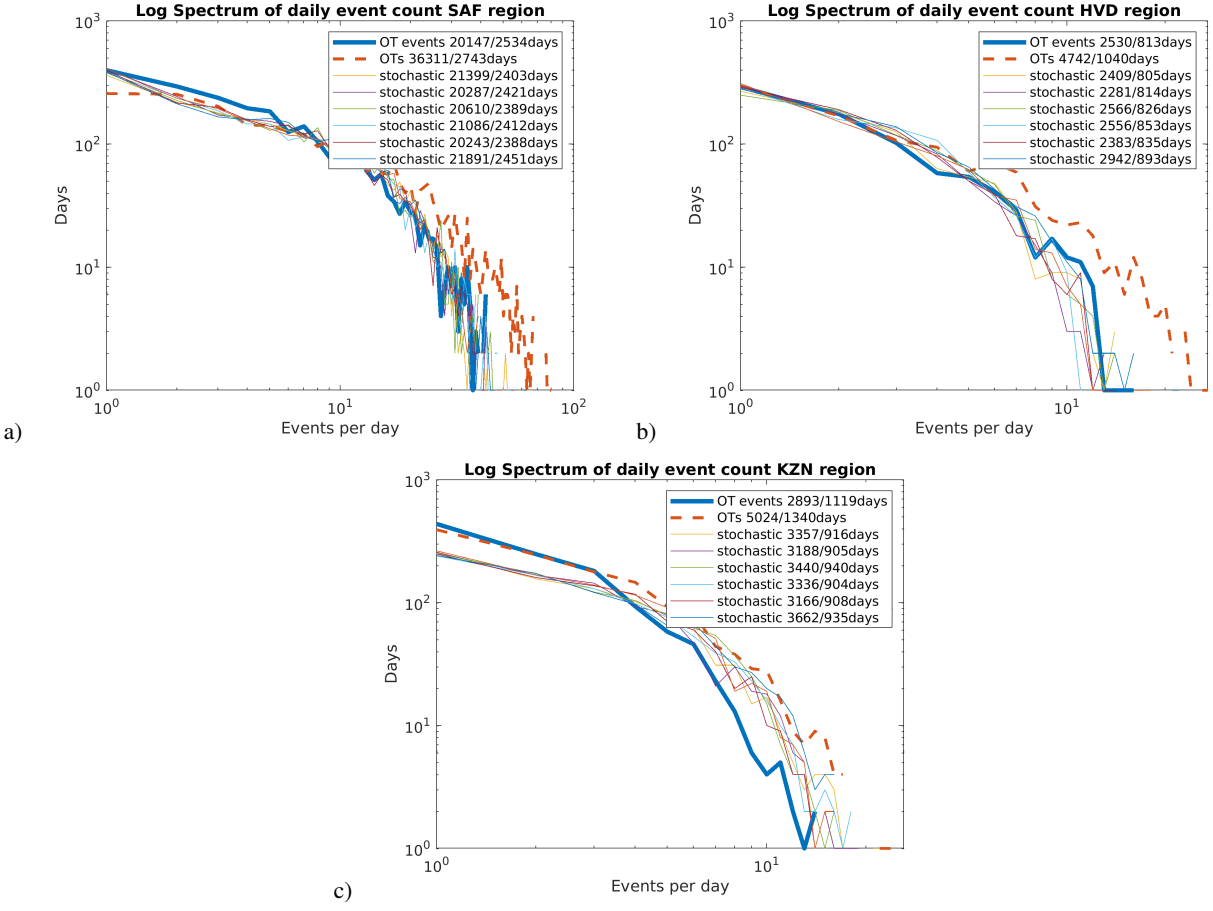

Figure 17. As Fig. 16, but comparing subsets of the stochastic event set to the historic OT event set (as well as the set containing events lasting only one time step) for each region. a) South Africa, b) Highveld, c) KwaZulu-Natal. Numbers indicate the total count and total number of days on which these occurred for each set.

sampling, is introduced to make risk calculations more efficient, reducing the event count by a factor of approximately ten. However, the most important events in terms of damage potential are over-represented to allow for adequate statistics (notably, computing damage at higher return periods reliably).

The newly introduced explicit modeling of the date requires that all events occurring on the same day need to be considered together. Consequently, daily aggregated damage potential (here: ellipse area times maximum hail size) is the relevant quantity for to rank event days by severity. The class thresholds correspond to the 50th, 80th, 95th, and 99th percentiles of severity, splitting the event set into 5 classes, of which 7.5, 2.5, 5, 10, 100 % were retained, respectively. To compensate, the retained events are attributed a higher frequency (default is once per event set period, e.g., 25 000 years), so the total damage potential is conserved.

https://doi.org/10.5194/nhess-2021-342
Preprint. Discussion started: 25 November 2021

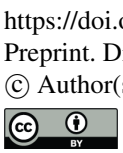

Natural Hazards and Earth System Sciences
Discussions

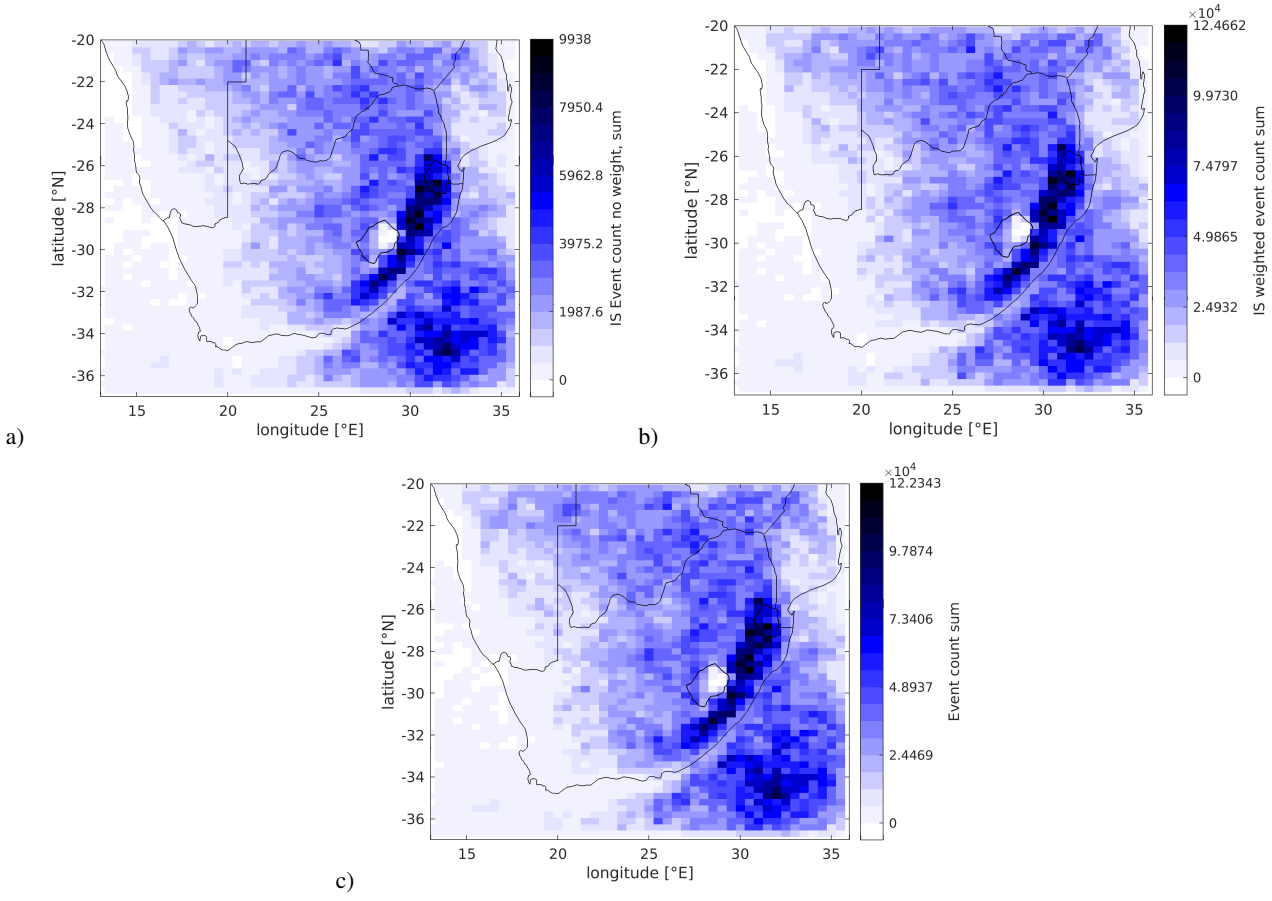

Figure 18. a: Number of events retained by the importance sampling, b: As a, but weighed by frequency, c: event frequency before importance sampling, showing very little difference.

The large differences in event frequency across South Africa mean that local statistics on, for example, hail damage or probable maximum loss for a 200-year return period, can rely on a much bigger sample in the hail hot spots of the country compared to the less hail-prone regions in the west. It is hence important to retain a minimum number of events in those low-hail regions, in practice at least one per 250-year batch (if one is present in the first place).

Figure 18 illustrates this point: part a) shows the distribution of events retained in the importance sampling, some areas in the west and far north have less than 50 events in a $0.5° \times 0.3°$ box (≈ 30 km in extent). As to be expected, when frequency weights are applied, the distribution corresponds to that of the full event set.

4.2 Footprint generation

Finally, the areas affected by hail and the corresponding hail size need to be determined for the stochastic events, forming a hail “footprint." Given the arbitrary paths of thunderstorms observed for the historic events, we chose to achieve this by a

https://doi.org/10.5194/nhess-2021-342
Preprint. Discussion started: 25 November 2021

Natural Hazards and Earth System Sciences
Discussions

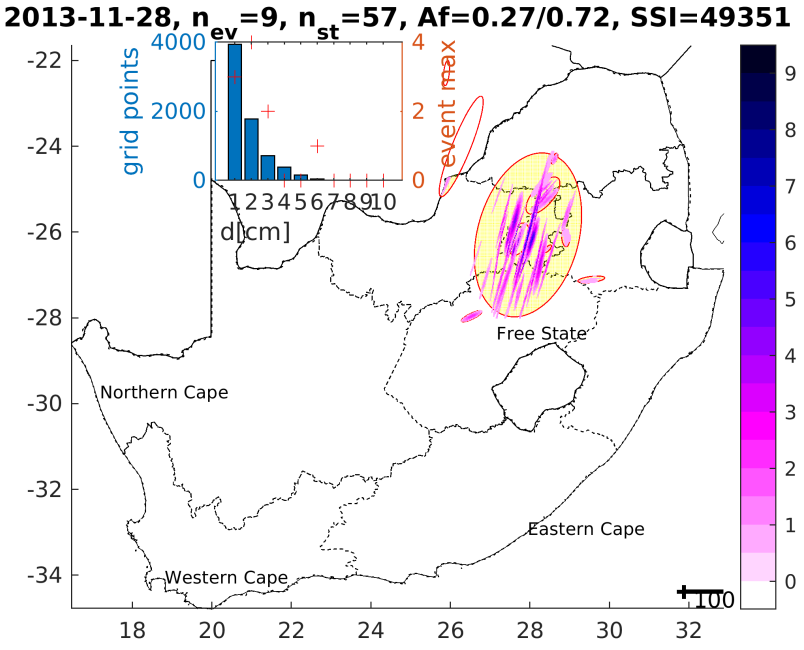

Figure 19. Example daily hail footprint generated with the model algorithm for events on 28 November 2013. Streaks cannot be expected to match historic observations, as they are located at random. The inset shows the maximum hail size distribution of pixels (blue) and events (red crosses).

randomized process of allocating ellipsoid hailstreaks within the event area. These are aggregated across all events of a day to form the daily hail footprint, which is applied to portfolios in the further stages of the risk model. The footprint catalog gives local information on hail occurrence and diameter for each day on a $2 \times 2\,\mathrm{km}^2$ grid covering continental South Africa.

The footprint generation algorithm attempts to mimic observed patterns of hailfall in an empirical way. A first streak is located in the center of the event, and its length, orientation and maximum hail diameter match those attributed to the event. Streak widths were chosen to approximate hailstreaks in ground- and radar-based studies (Stout et al., 1960; Changnon Jr, 1977; Kleinschroth, 1999; Schmidberger, 2018; Fluck et al., 2021), without strictly following observed distributions. An exponential distribution is assumed, with a mean width of 6 km, and a maximum of 20 km. Hail size decreases towards the streak's edges in a parabolic way, as proposed by Schmidberger (2018). This is deemed acceptable since actual hail patterns on the ground are largely uncertain across the world. In an iterative process, further streaks are added until the combined streak area covers the prescribed fraction of the event area. They are located randomly within the event area, and the possible event length decreases with each new streak. Streak orientation is varied by +/- 10° around the event orientation, while the maximum hail diameter of a streak decreases with distance from the event center. For illustration, Fig. 19 gives a sample of event hail streaks generated for events on the historic date 28 November 2013 (compare to the actual storm pattern in Fig. 7).

https://doi.org/10.5194/nhess-2021-342
Preprint. Discussion started: 25 November 2021

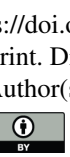

Natural Hazards and Earth System Sciences
Discussions
Open Access
EGU

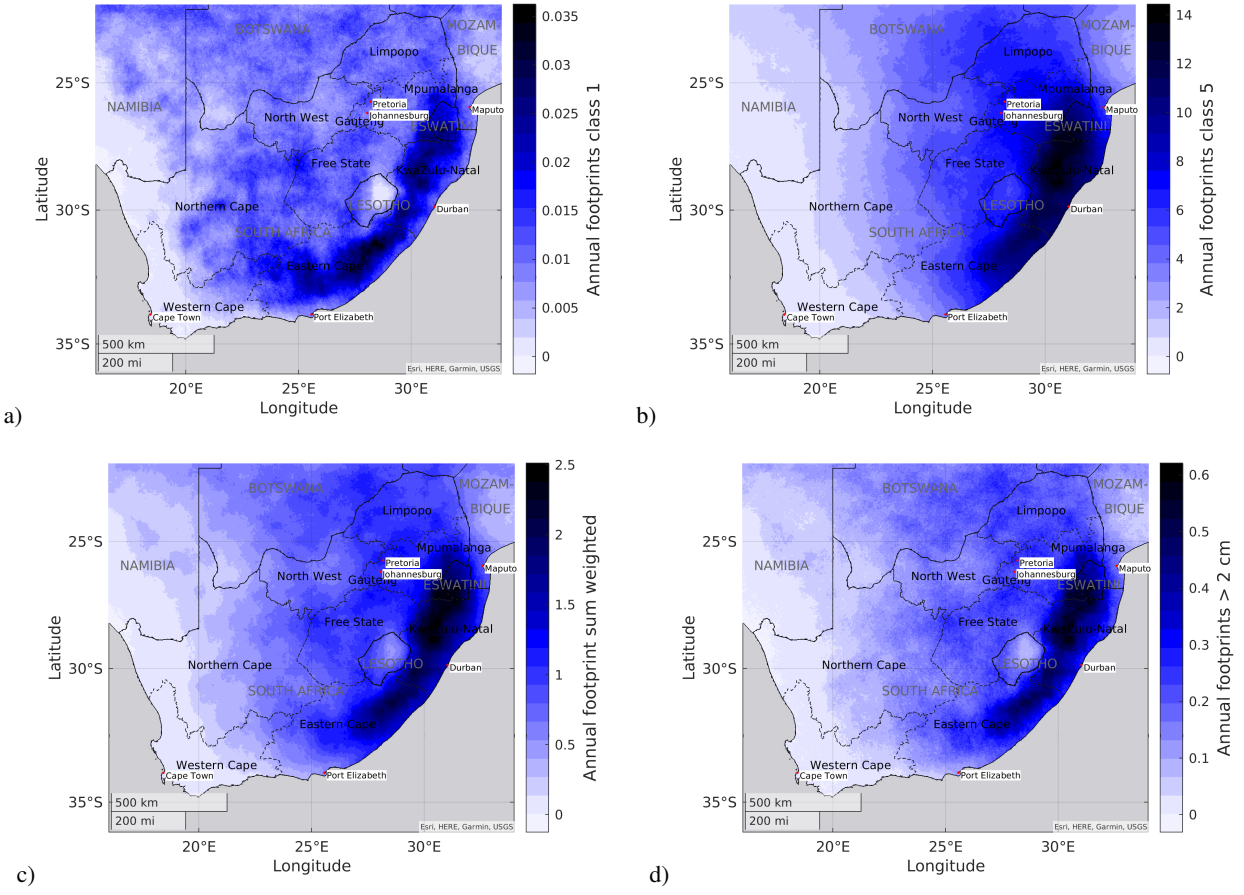

Figure 20. Number of events hitting a grid cell per year(a)–(b): for classes 1 and 5, respectively, (c): total, frequency-weighed, (d) as (c), but for hail diameter >2 cm.

Accumulating events over a time equivalent of 2 500 years, Fig. 20a and b show the number of events hitting each cell for a 10%-sample of the importance sampled event set, for the least and most severe class (1 and 5, respectively). Clearly, the footprint frequency over the Highveld and KwaZulu-Natal increases from class 1 to 5, whereas it decreases in the western half of the country. Consequently, hailstorms are relatively more often severe over the Highveld than other parts of the country, with important consequences on the financial risks associated with the peril. Figure 20c shows the accumulated, frequency-weighed annual sum of hail occurrences in the model and Fig. 20d the same occurrence for maximum hailstone diameters greater than 2 cm. We also note that the local 2 cm-hail count per year is about 2 in the KwaZulu-Natal maximum and around 1 in the Highveld and Gauteng regions, roughly in line with 0.81 normalized hail days per year in Held (1974).

Based on the local hail count and event set length, return periods, i. e. inverse frequencies, can be estimated for given hail diameter thresholds. Hail diameters for a fixed return period have then been calculated by linear interpolation between such thresholds fixed at 0.5 cm intervals. Summarizing the information contained in the event set, Fig. 21 shows the hail diameter

https://doi.org/10.5194/nhess-2021-342
Preprint. Discussion started: 25 November 2021

Natural Hazards and Earth System Sciences
Discussions
Open Access
EGU

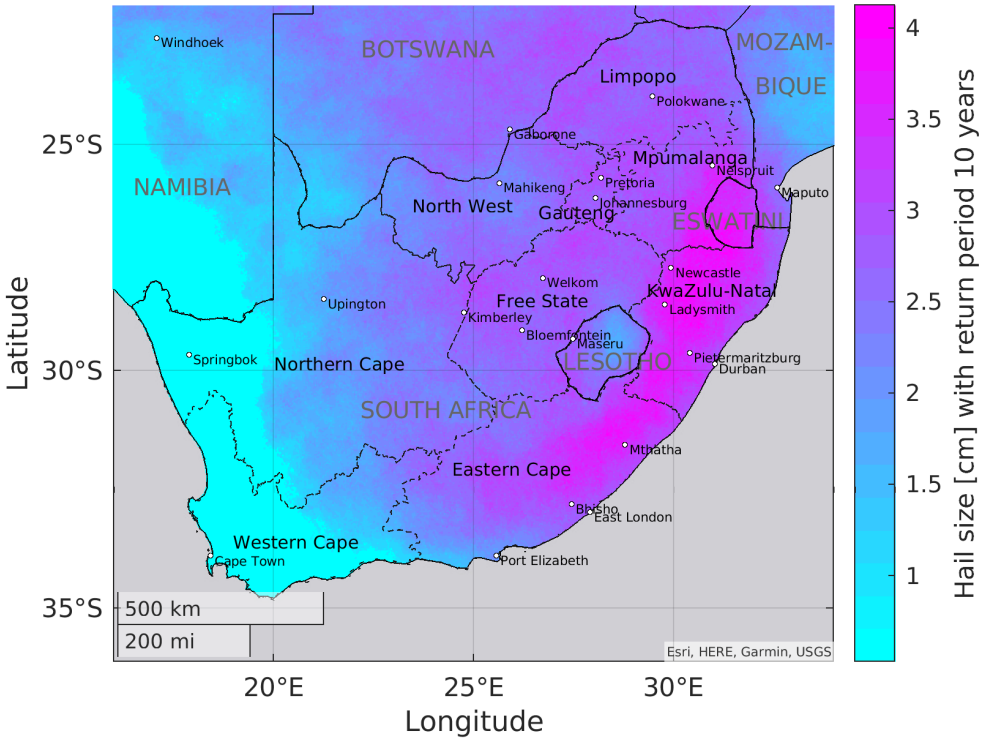

a)

Figure 21. Model-estimated maximum hail size occurring once in 10 years for grid cells across South Africa, computed as the lowest hail diameter class with a return period

that can be expected once per decade at a given location: In the most affected parts in the East, near Newcastle and Ladysmith, hailstones of around 4 cm are to be expected, followed by 3.5 cm for Pietermaritzburg, Mthatha or Nelspruit, 3.1 cm in Durban, 2.8 cm in the major cities of the Gauteng, but less than 2 cm in the western third of the country. Despite the uncertainty regarding the exact hail size – OT relation, this information has clear implications on the need for mitigation measures to reduce hail risk, such as roof cover robustness or covered parking of vehicles.

5 Conclusions

While the occurrence of hail is not captured by human spotter or hailpad observations in South Africa, space-borne observations of severe thunderstorms are sufficiently frequent and detailed to describe the nature of intense convection in the country quite accurately, from which the hail hazard can be derived. The diagram in Fig. 22 illustrates how data sources are combined in the model and processed to yield a set of event footprints representing 25 000 years of hail-generating convective storms based on the climate and weather of the period 2005-2018.

https://doi.org/10.5194/nhess-2021-342
Preprint. Discussion started: 25 November 2021

Natural Hazards and Earth System Sciences
Discussions

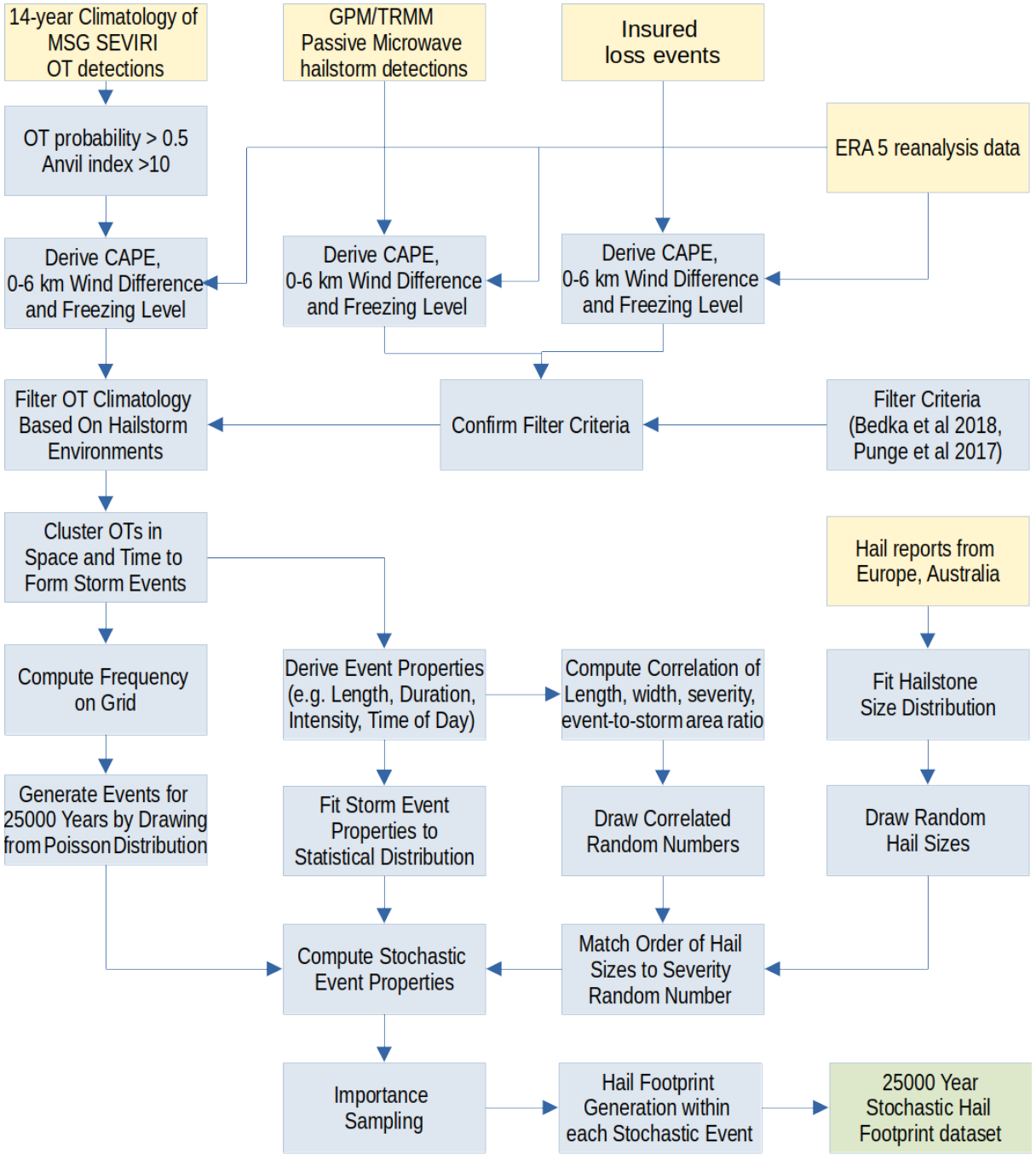

Figure 22. Diagram illustrating the functioning of the hail hazard model for South Africa

https://doi.org/10.5194/nhess-2021-342
Preprint. Discussion started: 25 November 2021

With the OT-based approach some scattered, short lasting hail episodes forming smaller hailstones may be missed, but are unimportant for the hail threat to insurance businesses, which are mostly concerned about major loss events. Another limitation of the OT approach is the difficulty to distinguish hail-producing from non-hail producing storms or identify the fraction of an individual storm's track in which it produces hail. While storm environments from reanalysis (Bedka et al., 2018; Punge et al., 2017) can help with the first task, they can hardly address the second.

Nonetheless, while the absolute number of hail days per year strongly depends on the minimum size of hail considered, findings are comparable to local hail reporting-based studies for the Gauteng region. However, there is disagreement with previous studies over the presence of a hail frequency maximum in the Lesotho mountains, absent in our study.

The combination of improved OT detection and advanced spatio-temporal clustering allows the determination of hail hazard zones much more precisely compared to the method used for the Willis European Hail Model (Punge et al., 2014). Regarding storm properties, in most instances exponential distributions have been replaced by GEV distributions, yielding a better fit to observations.

More importantly, the model is now capable of producing realistic spatio-temporal distribution of events, handling multiple events per day as well as their spatial spread and multi-year variability. By explicitly including the date as an event property, it has become possible to represent outbreaks with multiple events on a single day in a realistic way (see Fig. 17). Hence the increased financial risk of clusters with repeating severe storms (e.g., 11 and 28 November 2013 in Gauteng, Dyson et al. (2020); or in Germany on 27/28 July 2013, Kunz et al. (2018); Munich RE (2015)) is accounted for.

In addition, the footprint generation algorithm has been revised to predict hail only in a fraction of the event area, mimicking observed storms. This will assist the calibration of the exposure and vulnerability functions of the risk model and yield more accurate loss estimates. Finally, another addition compared to previous model versions is the time of day, which will allow to reflect daily changes in exposure, for example of parked cars, in the risk model.

Generally, the lack of accurate data of hail observations and damage reports limits the accuracy of hail hazard description (compared to, e.g., Europe, Púčik et al., 2019). The uneven distribution of population and wealth in the country complicates this matter further.

Author contributions. HJP, MK, SDB and KMB conceived the stochastic model and this study. KMB designed the OT detection algorithm, provided OT data, and suggested figures. MK supervised the model design and development. SDB developed the microwave hail detection algorithm and provided the corresponding data. KFI evaluated the OT algorithm against radar data and contributed Fig. 2. HJP analyzed the data and prepared the manuscript, with all co-authors providing critical feedback and helping shape the analysis and manuscript.

Competing interests. The authors declare they have no competing interests.

https://doi.org/10.5194/nhess-2021-342
Preprint. Discussion started: 25 November 2021

Natural Hazards and Earth System Sciences
Discussions
Open Access
EGU

Acknowledgements. The NASA Applied Sciences Disasters program award 18-DISASTER18-0008 supported the collaboration between NASA and KIT. Heinz Jürgen Punge is supported financially by WillisTowersWatson through the Willis Research Network. We thank ECMWF for providing ERA-5 reanalysis data and WillisTowersWatson for providing hail damage claims for sample events. We thank the European Severe Storms Laboratory (ESSL) and the Australian Bureau of Meteorology for providing hail report data. Credit is given to gadm.org und geonames.org for providing geodata used to produce the maps.

https://doi.org/10.5194/nhess-2021-342
Preprint. Discussion started: 25 November 2021

Natural Hazards and Earth System Sciences Discussions

References

Adler, R. F., Markus, M. J., and Fenn, D. D.: Detection of Severe Midwest Thunderstorms Using Geosynchronous Satellite Data, Mon. Wea. Rev., 113, 769–781, https://doi.org/https://doi.org/10.1175/1520-0493(1985)113<0769:DOSMTU>2.0.CO;2, 1985.

Admirat, P., Goyer, G. G., Wojtiw, L., Carte, E. A., Roos, D., and Lozowki, E. P.: A comparative study of hailstorms in Switzerland, Canada and South Africa, J. Clim., 5, 35–51, https://doi.org/https://doi.org/10.1002/joc.3370050104, 1985.

Allen, J. T., Tippett, M. K., and Sobel, A. H.: An empirical model relating U.S. monthly hail occurrence to large-scale meteorological environment, J. Adv. Model. Earth Sy., 7, 226–243, https://doi.org/https://doi.org/10.1002/2014MS000397, 2015.

Allen, J. T., Giammanco, I. M., Kumjian, M. R., Punge, H. J., Zhang, Q., Groenemeijer, P., Kunz, M., and Ortega, K.: Understanding Hail in the Earth System, Rev. Geophys., 58, e2019RG000 665, https://doi.org/https://doi.org/10.1029/2019RG000665, 2020.

Ayob, N.: Hail nowcasting over the South African Highveld, Master's thesis, North-West University (South Africa), 2019.

Bang, S. D. and Cecil, D. J.: Constructing a Multifrequency Passive Microwave Hail Retrieval and Climatology in the GPM Domain, J. Appl. Meteor. Climatol., 58, 1889–1904, https://doi.org/https://doi.org/10.1175/JAMC-D-19-0042.1, 2019.

Bang, S. D. and Cecil, D. J.: Testing Passive Microwave-Based Hail Retrievals Using GPM DPR Ku-Band Radar, J. Appl. Meteor. Climatol., 60, 255–271, 2021.

Bedka, K., Brunner, J., Dworak, R., Feltz, W., Otkin, J., and Greenwald, T.: Objective Satellite-Based Detection of Overshooting Tops Using Infrared Window Channel Brightness Temperature Gradients, J. Appl. Meteor. Climatol., 49, 181–202, https://doi.org/https://doi.org/10.1175/2009JAMC2286.1, 2010.

Bedka, K. M.: Overshooting cloud top detections using MSG SEVIRI Infrared brightness temperatures and their relationship to severe weather over Europe, Atmos. Res., 99, 175–189, 2011.

Bedka, K. M. and Khlopenkov, K.: A probabilistic multispectral pattern recognition method for detection of overshooting cloud tops using passive satellite imager observations, J. Appl. Meteor. Climatol., 55, 1983–2005, 2016.

Bedka, K. M., Allen, J. T., Punge, H. J., Kunz, M., and Simanovic, D.: A long-term overshooting convective cloud-top detection database over Australia derived from MTSAT Japanese advanced meteorological imager observations, J. Appl. Meteor. Climatol., 57, 937–951, 2018.

Berthet, C., Dessens, J., and Sanchez, J.: Regional and yearly variations of hail frequency and intensity in France, Atmos. Res., 100, 391–400, 2011.

Carte, A.: Hail damage to agriculture and its prevention, S. Afr. J. Sci., 73, 327–330, https://journals.co.za/content/sajsci/73/11/AJA00382353_5020, 1977.

Carte, A. E.: Features of Transvaal hailstorms, Quart. J. Roy. Meteor. Soc., 92, 290–296, https://doi.org/https://doi.org/10.1002/qj.49709239214, 1966.

Cecil, D. J.: Passive Microwave Brightness Temperatures as Proxies for Hailstorms, J. Appl. Meteor. Climatol., 48, 1281, https://doi.org/https://doi.org/10.1175/2009JAMC2125.1, 2009.

Changnon, S. A.: Hailfall Characteristics Related to Crop Damage, J. Appl. Meteor. Climatol., 10, 270 – 274, https://doi.org/10.1175/1520-0450(1971)010<0270:HCRTCD>2.0.CO;2, 1971.

Changnon Jr, S. A.: The scales of hail, J. Appl. Meteor., 16, 626–648, 1977.

Cintineo, J. L., Smith, T. M., Lakshmanan, V., Brooks, H. E., and Ortega, K. L.: An Objective High-Resolution Hail Climatology of the Contiguous United States, Wea. Forecasting, 27, 1235–1248, https://doi.org/https://doi.org/10.1175/WAF-D-11-00151.1, 2012.

https://doi.org/10.5194/nhess-2021-342
Preprint. Discussion started: 25 November 2021

Cooney, J. W., Bedka, K. M., Bowman, K. P., Khlopenkov, K. V., and Itterly, K.: Comparing Tropopause-Penetrating Convection Identifications Derived from NEXRAD and GOES over the Contiguous United States, J. Geophys. Res.: Atmos., 126, https://doi.org/https://doi.org/10.1029/2020JD034319, 2021.

de Coning, E., Gijben, M., Maseko, B., and van Hemert, L.: Using satellite data to identify and track intense thunderstorms in South and southern Africa, S. Afr. J. Sci., 111, 1 – 5, https://doi.org/https://doi.org/10.17159/sajs.2015/20140402, 2015.

Dotzek, N., Groenemeijer, P., Feuerstein, B., and Holzer, A. M.: Overview of ESSL's severe convective storms research using the European Severe Weather Database ESWD, Atmos. Res., 93, 575–586, https://doi.org/http://dx.doi.org/10.1016/j.atmosres.2008.10.020, 2009.

Dowdy, A. J., Soderholm, J., Brook, J., Brown, A., and McGowan, H.: Quantifying hail and lightning risk factors using long-term observations around Australia, J. Geophys. Res.: Atmos., n/a, e2020JD033 101–T, https://doi.org/https://doi.org/10.1029/2020JD033101, 2020.

Dyson, L. L., Pienaar, N., Smit, A., and Kijko, A.: An ERA-Interim HAILCAST hail climatology for southern Africa, Int. J. Climatol., n/a, 262–277, https://doi.org/https://doi.org/10.1002/joc.6619, 2020.

Farr, T. G., Rosen, P. A., Caro, E., Crippen, R., Duren, R., Hensley, S., Kobrick, M., Paller, M., Rodriguez, E., Roth, L., et al.: The shuttle radar topography mission, Rev. Geophys., 45, 2007.

Feng, Z., Leung, L. R., Liu, N., Wang, J., Houze Jr, R. A., Li, J., Hardin, J. C., Chen, D., and Guo, J.: A Global High-Resolution Mesoscale Convective System Database Using Satellite-Derived Cloud Tops, Surface Precipitation, and Tracking, J. Geophys. Res.: Atmos., 126, e2020JD034 202, 2021.

Fluck, E., Kunz, M., Geissbuehler, P., and Ritz, S. P.: Radar-based assessment of hail frequency in Europe, Nat. Hazards Earth Sys. Sci., 21, 683–701, 2021.

Garstang, M., Kelbe, B. E., Emmitt, G. D., and London, W. B.: Generation of Convective Storms over the Escarpment of Northeastern South Africa, Mon. Wea. Rev., 115, 429–443, https://doi.org/https://doi.org/10.1175/1520-0493(1987)115<0429:GOCSOT>2.0.CO;2, 1987.

Giaiotti, D., Nordio, S., and Stel, F.: The climatology of hail in the plain of Friuli Venezia Giulia, Atmos. Res., 67-68, 247–259, 2003.

Grieser, J. and Hill, M.: How to Express Hail Intensity—Modeling the Hailstone Size Distribution, J. Appl. Meteor. Climatol., 58, 2329–2345, https://doi.org/https://doi.org/10.1175/JAMC-D-18-0334.1, 2019.

Held, G.: Hail frequency in the Pretoria–Witwatersrand area during 1962 to 1972, Pure Appl. Geophys., 112, 765–776, https://doi.org/https://doi.org/10.1007/BF00876951, 1974.

Hersbach, H., Bell, B., Berrisford, P., Hirahara, S., Horányi, A., Muñoz-Sabater, J., Nicolas, J., Peubey, C., Radu, R., Schepers, D., Simmons, A., Soci, C., Abdalla, S., Abellan, X., Balsamo, G., Bechtold, P., Biavati, G., Bidlot, J., Bonavita, M., De Chiara, G., Dahlgren, P., Dee, D., Diamantakis, M., Dragani, R., Flemming, J., Forbes, R., Fuentes, M., Geer, A., Haimberger, L., Healy, S., Hogan, R. J., Hólm, E., Janisková, M., Keeley, S., Laloyaux, P., Lopez, P., Lupu, C., Radnoti, G., de Rosnay, P., Rozum, I., Vamborg, F., Villaume, S., and Thépaut, J.-N.: The ERA5 global reanalysis, Quart. J. Roy. Meteor. Soc., 146, 1999–2049, https://doi.org/https://doi.org/10.1002/qj.3803, 2020.

Heymsfield, A. J., Giammanco, I. M., and Wright, R.: Terminal velocities and kinetic energies of natural hailstones, Geophys. Res. Lett., 41, 8666–8672, 2014.

Junghänel, T., Brendel, C., Winterrath, T., and Walter, A.: Towards a radar-and observation-based hail climatology for Germany, Meteor. Z., 25, 435–445, https://doi.org/https://doi.org/10.1127/metz/2016/0734, 2016.

Khlopenkov, K. V., Bedka, K. M., Cooney, J. W., and Itterly, K.: Recent Advances in Detection of Overshooting Cloud Topsfrom Longwave Infrared Satellite Imagery, J. Geophys. Res.: Atmos., https://doi.org/https://doi.org/10.1029/2020jd034359, 2021.

Kleinschroth, S.: Untersuchungen über den möglichen Einfluss des Naturraumes auf Entstehung und Verlauf von Hagelgewittern am Beispiel Bayern und Baden-Württemberg, München (Diploma thesis, Ludwig-Maximilians-Universität München), 1999.

https://doi.org/10.5194/nhess-2021-342
Preprint. Discussion started: 25 November 2021

Kunz, M., Blahak, U., Handwerker, J., Schmidberger, M., Punge, H. J., Mohr, S., Fluck, E., and Bedka, K. M.: The severe hailstorm in southwest Germany on 28 July 2013: Characteristics, impacts and meteorological conditions, Quart. J. Roy. Meteor. Soc., 144, 231–250, 2018.

Kunz, M., Wandel, J., Fluck, E., Baumstark, S., Mohr, S., and Schemm, S.: Ambient conditions prevailing during hail events in central Europe, Nat. Hazards Earth Sys. Sci., 20, 1867–1887, 2020.

Leigh, R. and Kuhnel, I.: Hailstorm loss modelling and risk assessment in the Sydney region, Australia, Natural Hazards, 24, 171–185, 2001.

Mardia, K. V. and Zemroch, P. J.: Algorithm AS 86: The Von Mises Distribution Function, J. Roy. Stat. Soc. C.-Appl., 24, 268–272, http://www.jstor.org/stable/2346578, 1975.

Marion, G. R., Trapp, R. J., and Nesbitt, S. W.: Using Overshooting Top Area to Discriminate Potential for Large, Intense Tornadoes, Geophys. Res. Lett., 46, 12 520–12 526, https://doi.org/https://doi.org/10.1029/2019GL084099, 2019.

Melcón, P., Merino, A., Sánchez, J. L., López, L., and Hermida, L.: Satellite remote sensing of hailstorms in France, Atmos. Res., 182, 221–231, 2016.

Mroz, K., Battaglia, A., Lang, T. J., Cecil, D. J., Tanelli, S., and Tridon, F.: Hail-Detection Algorithm for the GPM Core Observatory Satellite Sensors, J. Appl. Meteor. Climatol., 56, 1939–1957, https://doi.org/https://doi.org/10.1175/JAMC-D-16-0368.1, 2017.

Munich RE: Severe convective storms and hail - Icy cricket balls from above, Available at: http://www.munichre.com/australia/australia-natural-hazards/australia-storm/hailstorm/index.html, Accessed on 25th November 2015, Munich RE, 2015.

Murillo, E. M. and Homeyer, C. R.: Severe hail fall and hailstorm detection using remote sensing observations, J. Appl. Meteor. Climatol., 58, 947–970, 2019.

Ni, X., Liu, C., Cecil, D. J., and Zhang, Q.: On the Detection of Hail Using Satellite Passive Microwave Radiometers and Precipitation Radar, J. Appl. Meteor. Climatol., 56, 2693–2709, https://doi.org/https://doi.org/10.1175/JAMC-D-17-0065.1, 2017.

Nisi, L., Hering, A., Germann, U., and Martius, O.: A 15-year hail streak climatology for the Alpine region, Quart. J. Roy. Meteor. Soc., 144, 1429–1449, 2018.

Olivier, J.: Hail in the Transvaal - some geographical and climatological aspects, Ph.D. thesis, "Rand Afrikaans University", 1990.

Palencia, C., Castro, A., Giaiotti, D., Stel, F., Vinet, F., and Fraile, R.: Hailpad-based research: A bibliometric review, Atmos. Res., 93, 664–670, 2009.

Perry, A.: Severe hailstorm at Grahamstown in relation to convective weather hazards in South Africa, Weather, 50, 211–214, https://doi.org/https://doi.org/10.1002/j.1477-8696.1995.tb06110.x, 1995.

Petty, G. W. and Bennartz, R.: Field-of-view characteristics and resolution matching for the Global Precipitation Measurement (GPM) Microwave Imager (GMI), Atmos. Meas. Tech., 10, 745–758, 2017.

Powell, C. L. and Burger, R. P.: The severe Gauteng hailstorms of 28 November 2013, in: Proc. 30st Ann. Conf. South African, Soc. Atmos. Sci., 01-02 October 2014, Potchefstroom, South Africa, pp. 54–57, 2014.

Prein, A. F. and Holland, G. J.: Global estimates of damaging hail hazard, Wea. Clim. Extremes, 22, 10–23, 2018.

Punge, H. and Kunz, M.: Hail observations and hailstorm characteristics in Europe: A review, Atmos. Res., 176, 159–184, 2016.

Punge, H., Bedka, K., Kunz, M., and Reinbold, A.: Hail frequency estimation across Europe based on a combination of overshooting top detections and the ERA-INTERIM reanalysis, Atmos. Res., 198, 34–43, 2017.

Punge, H. J., Bedka, K. M., Kunz, M., and Werner, A.: A new physically based stochastic event catalog for hail in Europe, Nat. Hazards, 73, 1625–1645, https://doi.org/https://doi.org/10.1007/s11069-014-1161-0, 2014.

https://doi.org/10.5194/nhess-2021-342
Preprint. Discussion started: 25 November 2021


Natural Hazards and Earth System Sciences Discussions

Punge, H. J., Bedka, K. M., Kunz, M., and Reinbold, A.: Hail frequency estimation across Europe based on a combination of overshooting top detections and the ERA-INTERIM reanalysis, Atmos. Res., 198, 34–43, https://doi.org/https://doi.org/10.1016/j.atmosres.2017.07.025, 2017.

Puskeiler, M., Kunz, M., and Schmidberger, M.: Hail statistics for Germany derived from single-polarization radar data, Atmos. Res., 178-179, 459 – 470, https://doi.org/https://doi.org/10.1016/j.atmosres.2016.04.014, 2016.

Púčik, T., Castellano, C., Groenemeijer, P., Kühne, T., Rädler, A. T., Antonescu, B., and Faust, E.: Large Hail Incidence and Its Economic and Societal Impacts across Europe, Mon. Wea. Rev., 147, 3901 – 3916, https://doi.org/10.1175/MWR-D-19-0204.1, 2019.

Sandmæl, T. N., Homeyer, C. R., Bedka, K. M., Apke, J. M., Mecikalski, J. R., and Khlopenkov, K.: Evaluating the Ability of Remote Sensing Observations to Identify Significantly Severe and Potentially Tornadic Storms, J. Appl. Meteor. Climatol., 58, 2569–2590, https://doi.org/https://doi.org/10.1175/JAMC-D-18-0241.1, 2019.

Scarino, B. R., Bedka, K., Bhatt, R., Khlopenkov, K., Doelling, D. R., and Jr., W. L. S.: A kernel-driven BRDF model to inform satellite-derived visible anvil cloud detection, Atmos. Meas. Tech., 13, 5491–5511, https://doi.org/https://doi.org/10.5194/amt-13-5491-2020, 2020.

Schmetz, J., Pili, P., Tjemkes, S., Just, D., Kerkmann, J., Rota, S., and Ratier, A.: An introduction to Meteosat second generation (MSG), Bull. Am. Meteor. Soc., 83, 977–992, 2002.

Schmidberger, M.: Hagelgefährdung und Hagelrisiko in Deutschland basierend auf einer Kombination von Radardaten und Versicherungsdaten, Ph.D. thesis, Institute of Meteorology and Climate Research, Karlsruhe Institute of Technology (KIT), https://publikationen.bibliothek.kit.edu/1000086012, 263 pp, 2018.

Sioutas, M., Meaden, T., and Webb, J. D.: Hail frequency, distribution and intensity in Northern Greece, Atmos. Res., 93, 526–533, 2009.

Smith, H., Wingfied, M., and Coutinho, T.: The role of latent Sphaeropsis sapinea infections in post-hail associated die-back of Pinus patula, Forest Ecol. Manag., 164, 177 – 184, https://doi.org/10.1016/S0378-1127(01)00610-7, 2002.

Smith, S. B., Reuter, G. W., and Yau, M.: The episodic occurrence of hail in central Alberta and the Highveld of South Africa: Research note, Atmos.-Ocean, 36, 169–178, 1998.

Stout, G., Blackmer, R., and Wilk, K.: Hail studies in Illinois relating to cloud physics, Physics of Precipitation, Geophys. Monogr, 5, 369–381, 1960.

Taszarek, M., Allen, J. T., Púčik, T., Hoogewind, K. A., and Brooks, H. E.: Severe convective storms across Europe and the United States. Part 2: ERA5 environments associated with lightning, large hail, severe wind and tornadoes, J. Climate, pp. 1–53, https://doi.org/https://doi.org/10.1175/JCLI-D-20-0346.1, 2020.

Visser, P.: The Insurance Institute of South Africa –Breakfast Session on HAIL, Tech. rep., The Insurance Institute of South Africa, Hyde Park, Gauteng, 2014.

Wilhelm, J., Mohr, S., Punge, H. J., Mühr, B., Schmidberger, M., Daniell, J. E., Bedka, K. M., and Kunz, M.: Severe thunderstorms with large hail across Germany in June 2019, Weather, 76, 228–237, https://doi.org/https://doi.org/10.1002/wea.3886, 2021.

Wingfield, M. J. and Swart, W. J.: Integrated management of forest tree diseases in South Africa, Forest Ecol. Manag., 65, 11 – 16, https://doi.org/10.1016/0378-1127(94)90253-4, 1994.

Zinner, T., Forster, C., De Coning, E., and Betz, H.-D.: Validation of the Meteosat storm detection and nowcasting system Cb-TRAM with lightning network data-Europe and South Africa, Atmos. Meas. Tech., 6, 1567, 2013.